130 Advancement in OCT
Sunday, May 01, 2016 1:30 PM–3:15 PM
Exhibit/Poster Hall Poster Session
Program #/Board # Range: 433–474/A0070–A0111
Organizing Section: Multidisciplinary Ophthalmic Imaging Group

Program Number: 433 **Poster Board Number:** A0070
Presentation Time: 1:30 PM–3:15 PM
OCT-based whole eye biometry system
Mircea Mujat[2], Ankit Patel[2], Gopi Maguluri[2], Nicusor V. Iftimia[2], James D. Akula[1], Anne B. Fulton[1], R D. Ferguson[2]. [1]Ophthalmology, Boston Children's Hospital, Boston, MA; [2]Biomedical Optical Technologies, Physical Sciences, Inc., Andover, MA.
Purpose: To demonstrate a new dual-conjugate, dual-band approach to whole eye optical biometry. The flexibility and utility of such a system for wide-field measurements and diagnostics far exceeding axial lengths and thicknesses, and IOL power calculations is anticipated to make it commercially viable in many research and clinical applications.
Methods: That system was based upon an ellipsoidal optical scanning/imaging design that produces near-normal incidence scans over large patches of the eye's surface for efficient profiling and corneal/scleral surface stitching. This method permits simultaneous imaging of pairs of ocular surfaces with respect to the scan pivot point (the system pupil), by integration of dual-conjugate optics. Coordinated dual-reference arms enable ranging to these two focal surfaces at precisely known locations with respect to the scan pivot, and to each other, on a single SDOCT spectrometer without imposing extreme requirements on the axial imaging range. Direct imaging of the eye through the reflective scan optics allows the system pupil/pivot location to be precisely positioned by the operator, while the eye's position and orientation are monitored by a camera and controlled by a fixation display.
Results: The method has been initially demonstrated with a single imaging system by changing the beam focus and the scanning pivoting point and measuring various eye surfaces sequentially. Typical results for large area scans of cornea, iris and top of lens, and retina are shown in Fig. 1.
Conclusions: Our preliminary corneal/scleral, lenticular and retinal imaging demonstrations (performed at safe light levels for retinal imaging under NEIRB human subjects protocols) have shown coordinated optical delays and focal conjugate zoom control produce high quality SDOCT images ranging throughout the whole eye. Simultaneous measurement of anterior and posterior ocular anatomic structures and surfaces, and their precise spatial relationship to each other over wide angles, is feasible with a two-channel, dual-conjugate non-contact optical ocular biometry system in the optically accessible regions of the eye.

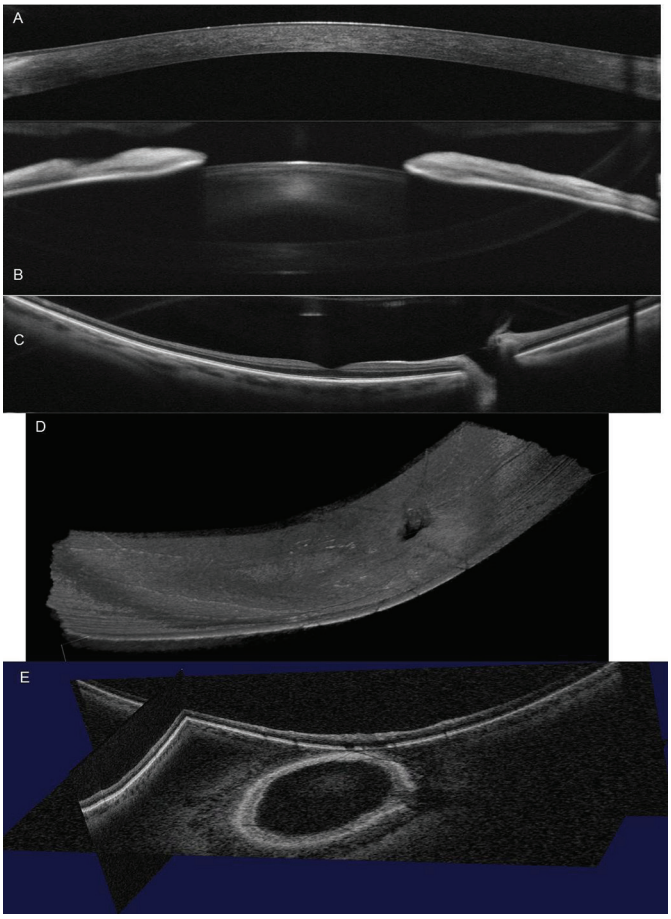

Figure 1. A: averaged image of the cornea; B: average image of the iris and top of the lens; C: average image of the retina; D: same optical configuration as C, configured as 3D raster, 50x100 deg (640 A-lines x 90 B-scans), corrected for eye motion and aligned; E: tangential and sagittal sections of the 3D data set.
Commercial Relationships: Mircea Mujat, Physical Sciences Inc.; **Ankit Patel**, Physical Sciences Inc. (C); **Gopi Maguluri**, Physical Sciences Inc.; **Nicusor V. Iftimia**, Physical Sciences Inc.; **James D. Akula**, None; **Anne B. Fulton**, None; **R D. Ferguson**, Physical Sciences Inc.
Support: NIH Grant - EY025895; Army Medical Research - W81XWH-12-C-0116

Program Number: 434 **Poster Board Number:** A0071
Presentation Time: 1:30 PM–3:15 PM
Truly simultaneous OCT of the anterior and posterior eye with full anterior chamber depth and 30° retinal field of view
Ryan P. McNabb[1], Brenton Keller[2], Joseph A. Izatt[2, 1], Anthony N. Kuo[1]. [1]Ophthalmology, Duke University Medical Center, Durham, NC; [2]Biomedical Engineering, Duke University, Durham, NC.
Purpose: Conventional OCT systems image only the anterior or posterior eye, not both. Newer OCT systems begin to do both but with compromises such as only imaging the fovea with the anterior segment or rapidly switching between the anterior and posterior eye. We describe here the development of an OCT system with truly simultaneous imaging of both the front and back of the eye capable of imaging the full anterior chamber depth and 30° on the retina (macula + optic nerve).

Methods: A swept source (λ_0=1045nm, $\Delta\lambda$=100nm, 200 kHz A-scan rate; Axsun, Inc.) OCT system with a polarization encoded, dual channel sample arm was designed to simultaneously image both the anterior and posterior eye with the requisite fields of view (Fig. A). The posterior eye pathlength was matched to the reference arm pathlength while the anterior eye pathlength was offset by one laser cavity length to take advantage of coherence revival [1]. A subject was consented under an IRB approved protocol. Repeated B-scans (1200 A-scans; 4128 samples per A-scan or 11.1mm of depth) were taken such that the fovea, optic nerve head, and anterior chamber were observed within each B-scan. The retina was encoded into the first 3mm of the scan with the anterior chamber occupying the remainder.

[1] A Dhalla, et al. Opt. Lett.37, 1883-1885 (2012)

Results: Figure B and C show 50 repeated and averaged B-scans acquired simultaneously from a healthy subject. The subject was wearing a contact and the corneal epithelial layer can be visualized (Fig. B). In the simultaneously acquired posterior scan, the retinal nerve fiber layer, outer plexiform layer, and the photoreceptor segment layer are visualized (Fig. C).

Conclusions: We have demonstrated an OCT system capable of truly simultaneous imaging of the both the anterior and posterior eye with sufficient field of view to see the full anterior chamber depth and the macula and optic nerve within one acquisition. This has important implications for clinical use of OCT to image the eye and for biometric applications.

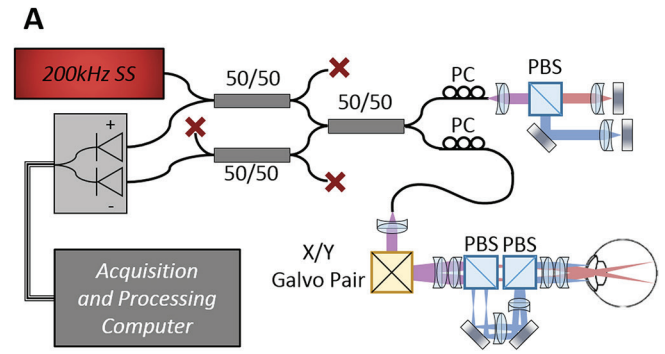

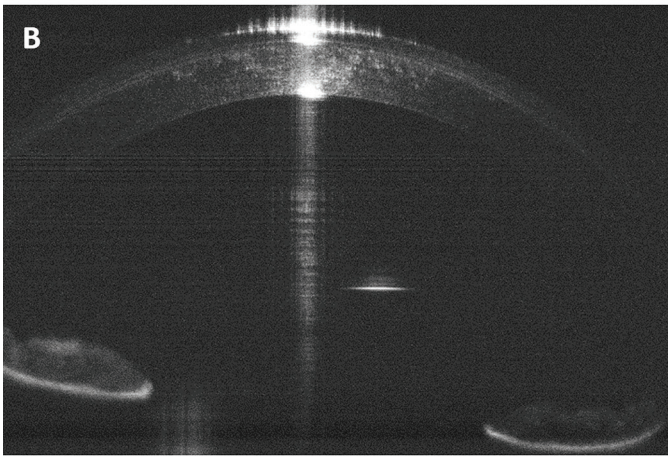

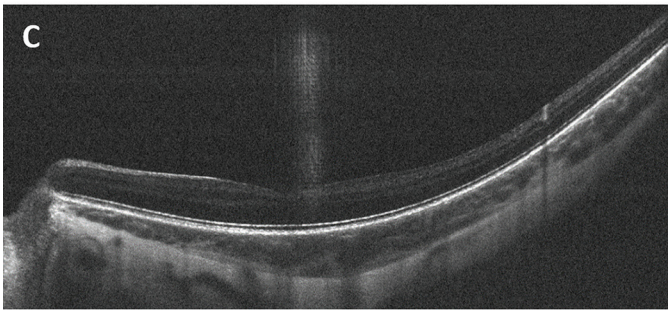

A) Simultaneous ocular anterior and posterior segment SSOCT imaging system schematic *B)* Anterior chamber of normal subject from 50 registered and averaged B-scans. There is a contact lens on the cornea and the corneal epithelial boundary is visible. *C)* Retina image acquired simultaneously with the anterior chamber scan in B (same 50 B-scans).

Commercial Relationships: Ryan P. McNabb; **Brenton Keller**, None; **Joseph A. Izatt**, Leica Microsystems (R), Leica Microsystems (P); **Anthony N. Kuo**, None
Support: NIH Grant R01EY024312

Program Number: 435 **Poster Board Number:** A0072
Presentation Time: 1:30 PM–3:15 PM

Automated analysis of retinal extracellular space using Optical Coherence Tomography. A non-invasive indirect identification of the sites of alterations of the Blood-Retinal Barrier

Torcato Santos[1], Jose G. Cunha-Vaz[1, 2]. [1]AIBILI, Coimbra, Portugal; [2]Faculty of Medicine, University of Coimbra, Coimbra, Portugal.

Purpose: Monitoring alterations of the Blood-Retinal Barrier (BRB) is presently performed by fluorescein angiography (FA), an invasive

method that uses an intravenous injection. We describe a new non-invasive method for localization and quantification of increases in retinal extracellular space, herein designated as OCT-Leakage using either Cirrus HD-OCT or AngioPlex (Carl Zeiss Meditec) devices. Increases in retinal extracellular space are surrogate indicators of breakdown of the BRB.
Methods: A semi-automated segmentation algorithm, able to identify 7 retinal layers, was applied to 48 eyes from 48 diabetic patients between 43 and 82 years of age (m±sd: 61.2±8.1 [years]) with normal Retinal Thickness (RT) (n=10), Subclinical Macular Edema (n=30) and Clinical Macular Edema (n=8). We also examined 25 eyes from 21 age matched healthy volunteers between 49 and 75 years of age (m±sd: 60.6±5.4 [years]). Optical reflectivity values were obtained for the full A-Scan within the retina and by retinal layer. The identification of Low Optical Reflectivity (LOR) sites corresponds to an increase of extracellular space. OCT-Leakage maps for full A-Scan within the retina and by retinal layer were thereafter generated to localize sites of increased extracellular space.
Results: Increases in Central Subfield RT in the eyes with subclinical and clinical macular edema were located mainly in the INL and OPL. These increases correlated well with the changes in LOR ratios, r=0.8 and r=0.6 ($p<0.01$) for INL and OPL, respectively. The OCT-Leakage maps identified well the sites of fluorescein leakage on FA. Furthermore, the location of the increases in extracellular space identified by the LOR ratios could be seen to predominate in different retinal layers in different eyes, indicating well the location of the increase of the extracellular space resulting from the breakdown of the BRB.
Conclusions: The method here described is able to detect and locate non-invasively the sites of leakage, i.e., alteration of the BRB in diabetic eyes. It offers an added value by identifying the changes occurring at different layers of the retina. OCT-Leakage location and quantification is thus able to complement OCT-Microangiography making it more likely to replace FA.
Commercial Relationships: Torcato Santos, None; **Jose G. Cunha-Vaz**
Clinical Trial: NCT01145599

Program Number: 436 **Poster Board Number:** A0073
Presentation Time: 1:30 PM–3:15 PM
Structure and vasculature of the human corneo-scleral limbus as imaged in-vivo with sub-micrometer axial resolution OCT
Kostadinka K. Bizheva[1, 2], Bingyao Tan[1], Erik Mason[1], Benjamin MacLellan[1], Lacey Haines[2], Ameneh Boroomand[3], Alexander Wong[3], Luigina Sorbara[2]. [1]Physics and Astronomy, University of Waterloo, Waterloo, ON, Canada; [2]School of Optometry and Vision Scieces, University of Waterloo, Waterloo, ON, Canada; [3]Systems Design Engineering, University of Waterloo, Waterloo, ON, Canada.
Purpose: To visualize in-vivo the microstructure and vasculature of the human corneo-scleral limbus by use of a sub-micrometer axial resolution OCT technology.
Methods: A sub-micrometer axial resolution, fiberoptic SD-OCT was developed for in-vivo imaging of the morphology and blood / lymph perfusion of the human corneo-scleral limbus. The UHR-OCT system utilizes a commercial supercontinuum light source, a custom filter to select the necessary spectral bandwidth and a 4096 pixel CCD. All optical and fiberoptic components of the system were specifically selected to sustain a spectral bandwidth > 260 nm centered at ~785 nm. The OCT system provides 0.95 µm axial and < 3µm lateral resolution in biological tissue and SNR of ~95 dB for 650 µW incident power. By utilizing different imaging protocols, both morphological and Doppler / OMAG images of the corneo-scleral limbus were acquired from healthy subjects and subjects with limbal abnormalities. The UHR-OCT images were processed with novel algorithms, developed by our research group, to further image resolution and contrast.
Results: Volumetric images of the human corneo-scleral limbus, acquired in-vivo with the new sub-micrometer resolution OCT system, allowed for visualization of the corneal epithelium and Bowman membrane's termination at the limbus, as well as the microstructure of the Vogt palisades. Overlapping Doppler OCT and IMAG images revealed the blood and lymph vasculature of the limbus. Both morphological and vascular changes were observed in cases of limbal abnormalities.
Conclusions: Sub-micrometer resolution OCT is capable of visualization and characterization of both the micro-structure and vasculature of the human corneo-scleral limbus.
Commercial Relationships: Kostadinka K. Bizheva, None; **Bingyao Tan**, None; **Erik Mason**, None; **Benjamin MacLellan**, None; **Lacey Haines**, None; **Ameneh Boroomand**; **Alexander Wong**, None; **Luigina Sorbara**, None
Support: CHRP (Candia Health Research Partnership) grant, NSERC Discovery grants

Program Number: 437 **Poster Board Number:** A0074
Presentation Time: 1:30 PM–3:15 PM
Long-Depth-Range Swept-Source OCT Instrument for Imaging Crystalline Lens Opacities
Ireneusz Grulkowski[1], Lukasz Cwiklinski[1], Silvestre Manzanera[2], Juan Mompeán[2], Pablo Artal[2], Maciej D. Wojtkowski[1]. [1]Faculty of Physics, Astronomy and Informatics, Nicolaus Copernicus University, Torun, Poland; [2]Laboratorio de Óptica, Universidad de Murcia, Murcia, Spain.
Purpose: In early cataracts, the crystalline lens presents some subtle opacifications causing an increase in scattering and a reduction in quality of vision. We have developed a long-range swept source OCT utilizing short external cavity wavelength tunable laser technology for *in vivo* three-dimensional (3-D) imaging of the crystalline lens to detect opacifications.
Methods: A high speed swept-source OCT instrument operating at 1050 nm for long-range imaging was developed and optimized for full anterior segment visualization. Imaging of the cornea and the crystalline lens at 50 kHz axial scan rate with 17 mm depth range was performed. OCT volumetric data sets consisting of 350x350 A-scans and covering 7x7 mm^2 area (iris area) were acquired. Different contrast parameters were explored in post-processing to effectively visualize the opacities in the crystalline lens. 3-D rendering of spatially resolved scattering within the lens were produced.
Results: We characterized the performance of the OCT system to minimize signal drop with depth (-6 dB at 10 mm depth) and achieve high sensitivity (102 dB). The swept light source used in the OCT system had enhanced coherence length leading to low signal drop. We obtained volumetric OCT tomograms spanning the depth of the entire anterior segment for 3-D visualization of the scattering properties of the crystalline lens. The opacities are characterized by enhanced scattering and generate shadows in cross-sectional images of the crystalline lens, which enables their effective mapping. Eyes with different types and degree of cataract severity were measured.
Conclusions: 3-D long-depth-range Swept-Source OCT enables volumetric visualization in vivo microstructural changes in the crystalline lens related to opacification. This instrument might be a useful tool in the evaluation and management of crystalline lens opacities in cataract patients.
Commercial Relationships: Ireneusz Grulkowski, None; **Lukasz Cwiklinski**, None; **Silvestre Manzanera**, None;

Juan Mompeán, None; **Pablo Artal**, None; **Maciej D. Wojtkowski**, None
Support: European Research Council SEECAT Grant ERC-2013-AdG-339228 & SEIDI Grant, Spain FIS2013-41237-R; Foundation for Polish Science TEAM Grant TEAM/2011-8/8; Polish Ministry of Science and Higher Education Grant IUVENTUS PLUS IP2014 014073

Program Number: 438 **Poster Board Number:** A0075
Presentation Time: 1:30 PM–3:15 PM
Anterior Segment Angiography with AngioPlex OCT Angiography on Cirrus 5000 SD-OCT
YINGJIAN WANG, Lin An, Patricia Sha, Venu Manne, Mary K. Durbin, Jochen Straub. CARL ZEISS MEDITEC, DUBLIN, CA.
Purpose: Optical Coherence Tomography Angiography (OCTA) is known to visualize retinal vasculature in the posterior segment of the eye with non-invasive, dye-less, technology. OCTA has not been investigated thoroughly to visualize the anterior segment. The goal of this study is to investigate the usability of OCTA to visualize anterior segment blood vessels of human eyes.
Methods: The commercially available ZEISS AngioPlex for retinal applications was adapted to visualize anterior segment eye blood vessels in human eyes. With an anterior segment lens adapter (Corneal add-on lens module, also commercially available), the system could achieve 4.2x4.2 mm field of view for high resolution imaging and 8.4x8.4 mm for low resolution imaging. The nasal and temporal conjunctiva and sclera adjacent to the limbus of human eyes were imaged.
Results: Anterior segment angiography was performed on 6 eyes of 3 normal subjects. For all 6 eyes, a detailed vasculature map was extracted from the adapted Cirrus AngioPlex. The imaging results of one example is demonstrated in Fig.1 and Fig.2. Fig.1 illustrates the corresponding area where the OCTA images was captured (the yellow square of Fig.1). Fig.2 is the OCTA results. Fig.2 (a) is the OCT intensity fundus image, which is obtained from integrating the OCT signal along the depth direction. Fig.2(b) is the corresponding OCT vasculature image. Fig.(c) and (d) are the B-scan structure and flow (red color in (d)) image of sclera, corresponding to the location marked by the light blue in Fig (a) and (b).
Conclusions: The Cirrus-5000's AngioPlex can be adapted to visualize anterior segment eye blood vessels, which may be useful for objective evaluation and monitoring progression of anterior neovascularization and vascular abnormalities in the future.

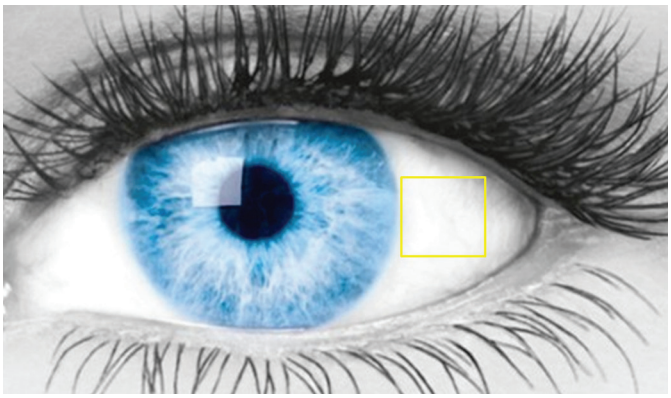

Figure 1: Schematic of Cirrus-5000 Anterior Segment AngioPlex scan on the human sclera

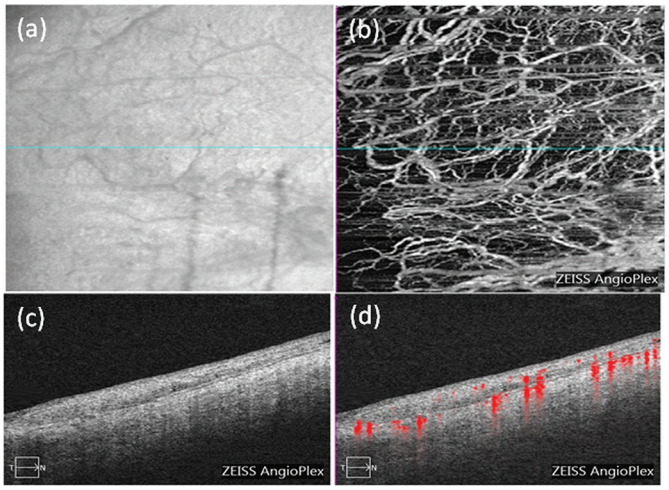

Figure 2: OCT angiography results of human sclera area obtained with Cirrus-5000 Anterior Segment AngioPlex prototype
Commercial Relationships: YINGJIAN WANG; **Lin An**, CARL ZEISS MEDITEC; **Patricia Sha**, CARL ZEISS MEDITEC (C); **Venu Manne**, CARL ZEISS MEDITEC; **Mary K. Durbin**, CARL ZEISS MEDITEC; **Jochen Straub**, CARL ZEISS MEDITEC

Program Number: 439 **Poster Board Number:** A0076
Presentation Time: 1:30 PM–3:15 PM
The Assessment of Henle Fiber Layer-Related Imaging Patterns on Directional OCT Scans of the Macula
Gabor M. Somfai[1, 2], Jing Tian[3], Delia DeBuc[3], Heinrich Gerding[1]. [1]Retinology Unit, Pallas Kliniken, Olten, Switzerland; [2]Department of Ophthalmology, Semmelweis University, Budapest, Hungary; [3]Bascom Palmer Eye Institute, University of Miami, Miller School of Medicine, Miami, FL.
Purpose: The segmentation of macular optical coherence tomography (OCT) scans is a valuable tool for the understanding of various retinal pathologies. There are, however, several artifacts potentially involved in the segmentation process, among them the typically hyperreflective Henle Fiber Layer (HFL), appearing as a part of the outer nuclear layer (ONL) under specific imaging conditions. The appearance of the HFL is dependent on the imaging beam entrance at the pupil and the resultant oblique scanning of the macula. As the HFL can overlap a significant part of the ONL and may thus also alter outer plexiform (OPL) measurements, there is a need to find a marker for this artifact on automated segmentation.
Methods: Directional OCT (D-OCT) technique was used that involves purposefully altering the entry position of the OCT beam. Imaging was carried out by Spectralis SD-OCT (Heidelberg Engineering, Heidelberg, Germany), using the "Dense" macular protocol. Seven eyes of five healthy subjects were involved in the study (1 male and 4 females, age 21-55 years). Three scans were taken of each eye with a central, temporal and nasal displacement of the imaging beam. The built-in segmentation algorithm of the Spectralis SD-OCT device was used and segmentation maps of the outer plexiform layer (OPL) were exported. The ratios of the superior vs. inferior and temporal vs. nasal ETDRS areas were calculated and compared by paired t-test.
Results: Imaging artifacts were observed as variable areas of increased thickness, depending on the scanning beam displacement and appearing on the contralateral side relative to the beam (i.e. temporal beam displacement resulting in a nasal artifact). Significant differences were observed with the temporal beam displacement in the comparisons of the inner-temporal vs. inner-nasal and the outer-

temporal vs. outer-nasal region ratios (inner-temporal/inner-nasal: 1.01±0.11 vs 0.59±0.19 and outer-temporal/outer-nasal: 0.99±0.11 vs 0.77±0.07, for the middle vs. the temporal beam placement, respectively, $p<0.05$ for both comparisons).
Conclusions: Our findings may facilitate the automatic detection of HFL artifacts during the automated segmentation of macular OCT volumes, while, at the same time, they may also help to understand the in vivo morphology of the photoreceptor and Müller cell axons.
Commercial Relationships: Gabor M. Somfai; **Jing Tian**, None; **Delia DeBuc**, None; **Heinrich Gerding**, None

Program Number: 440 **Poster Board Number:** A0077
Presentation Time: 1:30 PM–3:15 PM
Longitudinal change of macular, ganglion cell layer, and retinal nerve fiber layer thickness after vitrectomy: twelve-month observational study
Jung Yeul Kim[1, 2], Min Su Kim[2], Hyung bin Lim[2], Kyung sup Shin[2].
[2]Ophthalmology, Chungnam National University College of Medicine, Daejeon, Korea (the Republic of).
Purpose: We performed a *prospecitve, observational study* to analyze the longitudinal changes in the macular, ganglion cell–inner plexiform layer (GC-IPL), and peripapillary retinal nerve fiber layer (RNFL) thicknesses after vitrectomy.
Methods: Patients diagnosed with intraocular lens dislocation with no evidence of other vitreoretinal disease were analyzed. All of the patients underwent a conventional vitrectomy and intraocular lens trans-scleral fixation and followed for 12 months after vitrectomy. Using spectral domain optical coherence tomography (SD-OCT), we measured the thickness of the macular, GC-IPL, and peripapillary RNFL in the vitrectomized and fellow control eyes before surgery and at 1, 3, 6, and 12 months after surgery. We evaluate the change of thickness of retina in OCT measurements after surgery with the passage of time.
Results: There were no significant differences in the thickness of the macular, GC-IPL, and peripapillary RNFL using OCT between the study and fellow eyes from baseline. Postoperative central macular thickness did not show significant differences compared to baseline values. The mean GC-IPL thickness was increased at 1 month after surgery from baseline ($p=0.038$), but there were no significant differences at 3 months postoperatively. The mean RNFL thickness was significantly increased at 1 month ($p=0.001$) and 3 months ($p=0.011$) after vitrectomy from baseline, but there were no differences 6 months postoperatively. The mean foveal, GC-IPL and RNFL thicknesses of the study eye compared to the fellow eye were significantly increased at 1 month ($p=0.034$), at 1 month ($p=0.028$), and at 1 ($p=0.015$) to 3 months ($p=0.039$) after surgery, respectively. No significant differences in intraocular pressure and all disc parameters were found between study and fellow eyes during a follow-up of 12 months after surgery.
Conclusions: Transient increase of both macular and GC-IPL thicknesses was observed at 1 month following vitrectomy, and the postoperative RNFL thickness was increased until 3 months after surgery and thereafter, it returned to the preoperative level. There was no significant change in IOP and all disc parameters before and after surgery. These findings should be considered in the process of analyzing the retinal layer thickness obtained from OCT in patients with a history of vitrectomy.
Commercial Relationships: Jung Yeul Kim, None; **Min Su Kim**, None; **Hyung bin Lim**, None; **Kyung sup Shin**, None

Program Number: 441 **Poster Board Number:** A0078
Presentation Time: 1:30 PM–3:15 PM
Wide-field Swept Source OCT en-face image montages in healthy eyes
Jochen Straub, Conor Leahy, Jennifer Y. Luu. Carl Zeiss Meditec, Inc., Dublin, CA.
Purpose: To compare two alternative methods of acquiring and montaging Swept Source OCT (SS-OCT) en-face images of the human retina to achieve wide-field structural OCT en-face images.
Methods: The study was performed on three healthy dilated eyes using a ZEISS SS-OCT (ZEISS, Dublin, CA) prototype with an instantaneous optical field of view of 60degrees and a 100kHz swept source laser at 1050nm. The system has a scan depth of 3.0mm, a lateral resolution of 20microns, and an axial resolution of 5.5microns. Cube scans were taken over a 9x9mm and 12x12mm area with 500x500 and 512x512 A-scans respectively. The subjects' fixation was controlled using the internal fixation target. The ZEISS SS-OCT prototype provides retina tracking at 20Hz tracking speed.
Method 1: acquisition of 9 cube scans in a 3x3 pattern, using 9x9mm cubes; Method 2: acquisition of 4 cube scans in a 2x2 pattern, using 12x12mm cubes. After acquisition, the scans were exported and retinal montages created using an intelligent, semi-automated image stitching and blending algorithm.
Results: Images were acquired on three healthy eyes. For each eye we acquired nine OCT 9x9mm volumes and four 12x12mm volumes. Acquisition of the images took less than 10 minutes for nine acquisitions (method 1) and less than 5 minutes for four acquisitions (method 2). Patient alignment had to be corrected between individual cube acquisitions. The resulting montages cover an area of approximately 18x18mm using method 1 and approximately 21x21mm using method 2.
Conclusions: Montaging of structural OCT images allows for the creation of a large field-of-view OCT en-face image. Montages up to approximately 21x21mm were demonstrated.

Montage of nine OCT en-face images of a healthy human eye using the ZEISS SS-OCT prototype. Resulting field of view is approximately 18x18mm.

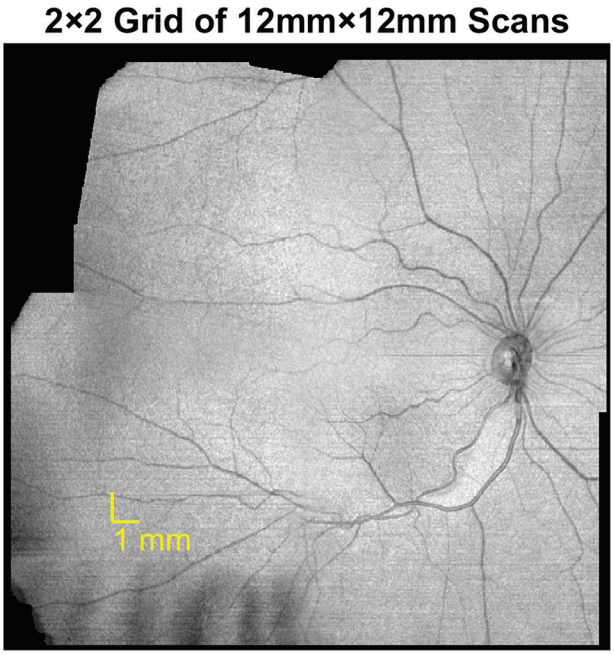

Montage of four OCT en-face images of a healthy human eye using the ZEISS SS-OCT prototype. Resulting field of view is approximately 21x21mm.

Commercial Relationships: Jochen Straub, Carl Zeiss Meditec, Inc.; **Conor Leahy**, Carl Zeiss Meditec, Inc.; **Jennifer Y. Luu**, Carl Zeiss Meditec, Inc.

Program Number: 442 **Poster Board Number:** A0079
Presentation Time: 1:30 PM–3:15 PM

Ultrawide-field OCT angiography with a 200kHz swept-source OCT system

Gangjun Liu, Jie Wang, Miao Zhang, Yali Jia, David Huang. Casey Eye Institute, Portland, OR.

Purpose: To demonstrate high-definition wide-field angiographic imaging of the human retina.

Methods: : A 200 kHz swept-source OCT system was developed using a tunable laser (Axsun, Inc.) operating at 1044 nm central wavelength. The laser has a tuning range of 104 nm, which provided an axial resolution of 5.7 microns full-width-half-maximum in tissue. The sample arm included a slit-lamp base, a chin rest, an iris camera, a pico-projector fixation target, and an electrically tunable lens for rapid focusing. The k-clock frequency was electronically doubled to increase the axial imaging range from 3.5 mm to 7.0 mm. A split-spectrum algorithm that combines both phase and amplitude information was used for angiographic calculation.

Results: Using only 2 B-frames at each location, high-definition (10~15 micron sampling interval) OCT angiography could be captured over 8x8mm or 10x6mm areas in 4 seconds. By montaging four 10x6mm scans, an ultrawide-field OCT angiography with 10x21 mm (35x70°) field of view was demonstrated (Fig. 1). The scan location was controlled by moving the fixation target using the pico-projector. The total imaging time for ultrawide field of view can be accomplished in 15 minutes.

Conclusions: By using a highly efficient angiography algorithm and a fast OCT system, wide-field OCT angiography could be achieved without sacrificing sampling density or extending acquisition time. Ultrawide field of view can be realized by montaging a few wide-field scans.

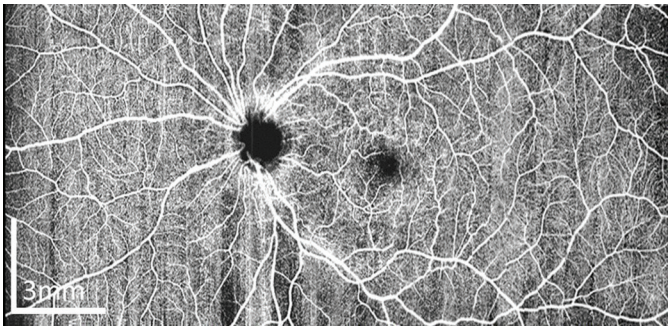

An ultrawide-field OCT angiography with 10x21 mm (35x70°) field of view. The angiographic image was obtained by montaging four 10x6mm (800 x 400 points) scans.

Commercial Relationships: Gangjun Liu, None; **Jie Wang**, None; **Miao Zhang**, None; **Yali Jia**, Optovue, Inc (P), Optovue, Inc (F); **David Huang**, Carl Zeiss Meditec, Inc. (P), Optovue, Inc (F), Optovue, Inc (P), Optovue, Inc (R), Optovue, Inc (I)

Support: Supported by Oregon Health & Science Foundation, DP3 DK104397, R01 EY024544, R01 EY023285 and P30 EY010572, and an unrestricted grant from Research to Prevent Blindness.

Program Number: 443 **Poster Board Number:** A0080
Presentation Time: 1:30 PM–3:15 PM
Single volume widefield retinal and choroidal OCT angiography of patients with MHz-OCT over 45° field of view
Jan Philip Kolb[1, 2], Thomas Klein[2], Kathrin J. Mohler[2], Wolfgang Wieser[2], Aljoscha S. Neubauer[3], Marcus Kernt[3], Anselm Kampik[3], Armin Wolf[3], Robert Huber[1]. [1]Institute for Biomlocular Optics, University of Lubeck, Luebeck, Germany; [2]Physics, University of Munich, Munich, Germany; [3]Ophthalmology, University of Munich, Munich, Germany.
Purpose: To investigate single volume OCT angiography of the retina and choroid in patients over a wide field of view of 45° (~13.5mm) with data captured by a MHz-OCT.
Methods: 45 patients diagnosed with various diseases including but not limited to AMD, diabetic retinopathy and macula edema were imaged with an OCT angiography protocol of a widefield MHz-OCT. This is a custom swept-source OCT device based on a Fourier-domain mode-locked laser source with 1050nm central wavelength and a depth scan rate of 1.68MHz, which is about 16 times faster than even the latest commercial swept-source OCT devices. Therefore, an OCT angiography protocol with 5x(1600x320) A-scans over 45° field of view took only 2.18s total acquisition time. In post processing, the RPE was automatically detected and angiograms of the retina (see fig. 1B) and the upper 40µm of the choroid (see fig. 1C) were computed by calculating the speckle variance of five consecutive B-scans taken at the same location. The optical nerve head (ONH) was assigned to the retina as RPE segmentation is not possible in this region.
Results: Single volume OCT angiography over a 45° field of view in patients is feasible and highlights retinal vessels, which are not visible in a regular enface images. Still, there are some challenges remaining: Shadowing due to eye lids and lashes and the pupil require careful alignment of the patient. B-scans with involuntary motion of the patient need to be filtered, but due to the high acquisition speed of the MHz-OCT this should be less critical than with a standard OCT. Moreover, the resolution in y-direction of 42µm given by density of B-scans seems to be too low to resolve very fine vessels.
Conclusions: OCT angiography with a MHz-OCT over 45° field of view with single volume acquisition in patients could be demonstrated for the first time. For future measurements the scan protocol should include a larger number of B-scans to improve the resolution in y-direction. Additionally, a more advanced processing of the data like SSADA could enhance the vessel contrast further.

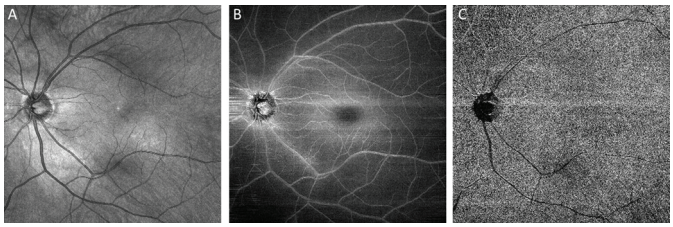

A) EnFace projection of OCT dataset from a 43 year old male patient showing 45° field of view. B) OCT Angiogram from the same dataset as A of the retina and ONH.C) OCT angiogram of the same dataset as A of the upper 40µm of the choroid.
Commercial Relationships: Jan Philip Kolb; **Thomas Klein**, None; **Kathrin J. Mohler**, None; **Wolfgang Wieser**, None; **Aljoscha S. Neubauer**, None; **Marcus Kernt**, None; **Anselm Kampik**, None; **Armin Wolf**, None; **Robert Huber**, None
Support: Emmy Noether program of the German Research Foundation (DFG – HU 1006/2-1), European Union projects FUN-OCT (FP7 HEALTH, contract no. 201880) and FDML-Raman (FP7 ERC, contract no. 259158), Freunde und Förderer der Augenklinik München e.V.
Clinical Trial: http://apps.who.int/trialsearch/default.aspx, DRKS00005173

Program Number: 444 **Poster Board Number:** A0081
Presentation Time: 1:30 PM–3:15 PM
OCT Angiography of the Human Choriocapillaris at 1.7M A-scans/second
Justin V. Migacz[2], Iwona M. Gorczynska[1, 2], Ravi S. Jonnal[2], Robert J. Zawadzki[2], John S. Werner[2]. [1]Physics, Astronomy and Informatics, Nicolaus Copernicus University, Torun, Poland; [2]Ophthalmology and Vision Science, University of California at Davis, Sacramento, CA.
Purpose: Optical coherence tomography angiography (OCTA) is an emerging tool for imaging vasculature in the healthy and diseased retina. Because image acquisition usually takes several seconds, involuntary saccadic movements of the eye create skew distortions and discontinuities in the resulting images, leading to an inaccurate representation of the vessel network. This is a significant problem when imaging the smallest vessels of the choriocapillaris. We have designed and constructed a small field of view (5x5 degrees), raster-scanning swept-source OCT system capable of imaging the human retina and choroid at 1.7 million axial scans per second, which is the fastest speed of any ophthalmic OCT system and about 20 times faster than commercial systems. With this extraordinarily high imaging speed, we are able to capture high-quality vessel maps of the choriocapillaris with a dramatic reduction of motion artifacts and distortions.
Methods: Our custom OCT system used a commercial swept-source laser (OptoRes GmbH, Munich, Germany, λ=1060 nm, $\Delta\lambda$=80 nm) with a sweep repetition rate of ~1.7MHz. The optical power of the OCT light beam on the cornea was 1.8mW. Single volumes spanned ~0.7x1.5mm on the retina and images of multiple locations were acquired, and tiled in post-processing. Angiograms were rendered from the volumetric data using multiple processing algorithms, including the phase-variance and amplitude decorrelation methods.
Results: In cross-sectional intensity images, motion of blood was visible in the retinal vascular plexi and choroidal layers, with the high frame rate permitting observation of the passage of small (5–10µm) objects in the vessels. High-contrast angiograms of the retina were generated, such as the ones shown in Figures 1 and 2. These images show clearly the microscopic structure of the choriocapillaris, and were acquired in a fraction of the time of most other OCTA systems.
Conclusions: Our 1.7M A-scan/sec acquisition speed OCTA system is capable of producing choriocapillaris images with high contrast, higher than when averaging multiple slower volumes. These images can facilitate our understanding of the role played by microscopic vascular structures in diseases of the outer retina.

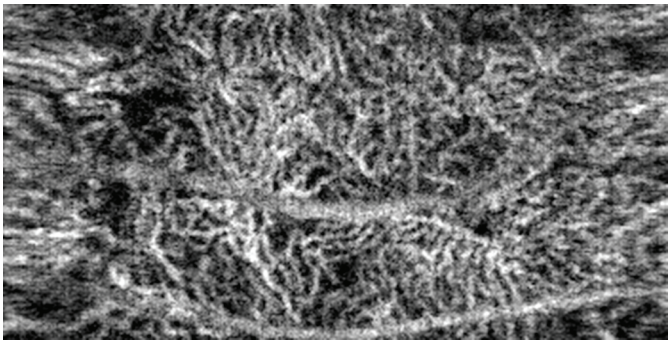

Choriocapillaris at 8° nasal, 2.5° superior from the fovea

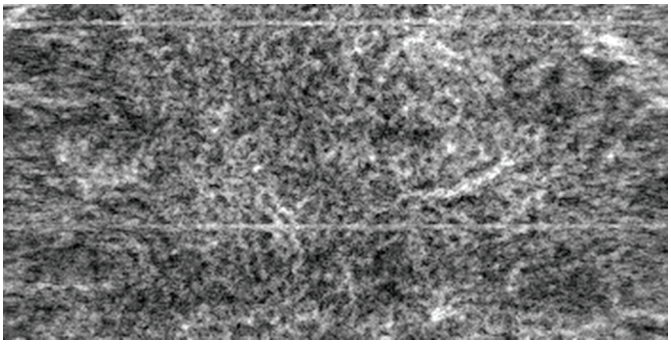

Choriocapillaris at fovea

Commercial Relationships: Justin V. Migacz; **Iwona M. Gorczynska**, None; **Ravi S. Jonnal**, None; **Robert J. Zawadzki**, None; **John S. Werner**, None
Support: NEI Grant EY024239

Program Number: 445 **Poster Board Number:** A0082
Presentation Time: 1:30 PM–3:15 PM
Widefield Swept-Source Optical Coherence Tomography Angiography

Anoush Shahidzadeh[1], Alice Y. Kim[1], Hassan A. Aziz[1], Mary K. Durbin[2], Carmen A. Puliafito[1], Amir H. Kashani[1].
[1]Ophthalmology, University of Southern California, Los Angeles, CA; [2]Research & Development, Carl Zeiss Meditec, Dublin, CA.

Purpose: To evaluate the benefits and limitations of wide-angle swept source optical coherence tomography angiography (SS-OCTA) 12x12mm scans compared to spectral domain OCTA (SD-OCTA) 6x6mm scans.

Methods: Patients with possible extramacular retinal pathology were recruited and imaged at the USC Eye Institute with prototype Cirrus SD-OCTA and SS-OCTA devices (Carl Zeiss Meditec, Dublin, CA). The SD-OCTA used a wavelength of 840 nm with scan speed of 68kHz, whereas the SS-OCTA used a wavelength of 1060nm with scan speed of 100kHz. Both devices had an axial resolution of 5um and lateral resolution of 15um. At least one 6x6mm SD-OCTA scan and one 12x12mm SS-OCTA scan centered on the fovea were taken for each study eye. Average acquisition time, quality of images, and ability to detect extramacular pathologies were assessed and compared within each scan frame. The structural en face images accompanying each OCTA scan were used to validate the quality of scans chosen for comparisons.

Results: Nine subjects (11 eyes) with the following retinal pathologies were included in this study: ERM, diabetic retinopathy, macular edema, vitreomacular traction, dry age related macular degeneration, optic neuritis, hypertensive retinopathy, and vitreous hemorrhage. Seven eyes demonstrated significant extramacular pathology in the 12x12mm SS-OCTA scans that was not visible in 6x6mm SD-OCTA scans. Average acquisition times for SD- and SS-OCTA images were approximately 4 seconds and 5-12 seconds, respectively, depending on fixation. Overall, there was no qualitative difference in scanning performance or patient experience between either device. In addition, overall quality of angiographic information in SS-OCTA images was qualitatively similar to SD-OCTA.

Conclusions: SS-OCTA systems can provide additional angiographic information in a quick, non-invasive, and convenient way analogous to SD-OCTA systems without significant compromise in performance. Larger fields of view allow for easier identification of extramacular pathologies that may be clinically relevant.

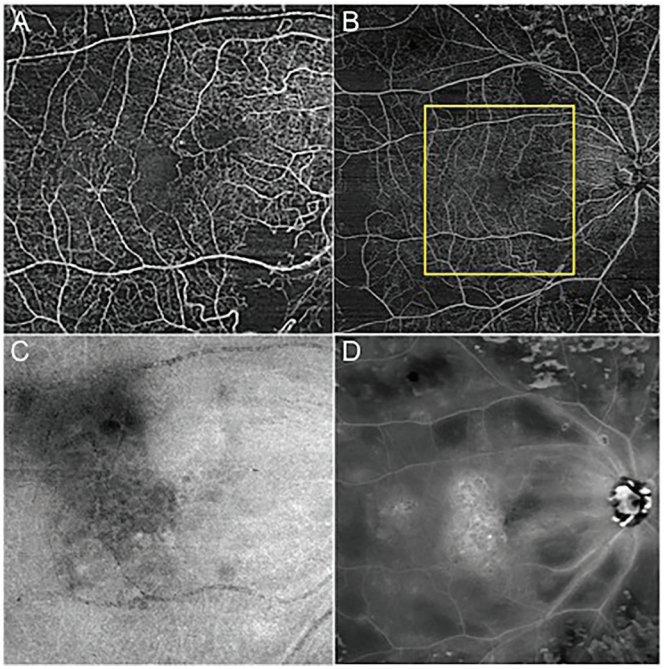

6x6mm SD- and 12x12mm SS-OCTA images of the left eye of a 38-year-old male with proliferative diabetic retinopathy and macular edema previously treated with laser and injections. (A) SD- and (B) SS-OCTA scans centered around the fovea and there structural en face images below (C, D respectively). The yellow box in (B) shows the area encompassed by the 6x6mm SD-OCTA scan.

Commercial Relationships: Anoush Shahidzadeh; **Alice Y. Kim**, Carl Zeiss Meditec, Inc. (F); **Hassan A. Aziz**, Carl Zeiss Meditec, Inc. (F); **Mary K. Durbin**, Carl Zeiss Meditec, Inc.; **Carmen A. Puliafito**, Carl Zeiss Meditec, Inc. (F); **Amir H. Kashani**, Carl Zeiss Meditec, Inc. (R), Carl Zeiss Meditec, Inc. (C), Carl Zeiss Meditec, Inc. (F)
Support: Research to Prevent Blindness

Program Number: 446 **Poster Board Number:** A0083
Presentation Time: 1:30 PM–3:15 PM
Automated Retinal Segmentation for Widefield OCT, with applications to OCT Angiography

Giovanni Gregori, Philip J. Rosenfeld, Luiz Roisman, Karen B. Schaal. Ophthalmology, Bascom Palmer Eye Institute, Miami, FL.

Purpose: The goal was to produce a new fast, robust algorithm capable of segmenting retinal layers from OCT images. The algorithm is intended for use on the very large datasets and field of views acquired using a widefield Swept Source OCT prototype in clinical situations, for the study of eyes with significant pathologies.

This is particularly important for applications in OCT angiographic imaging where visualization of blood flow within the appropriate anatomical regions is crucial for the appropriate clinical interpretation of images.
Methods: A new fully automated algorithm was used to segment several retinal layers from both OCT intensity and OCT angiography datasets. In particular, we studied images obtained from a prototype 100-kHz SS-OCT instrument (Carl Zeiss Meditec, Dublin, CA) with a central wavelength of 1,050 nm. This instrument is capable of acquiring both intensity and angiography scans over retinal areas up to 12x12mm (512x512 to 1000x1000 cubes for intensity scans, 450x450 cubes for OCT angiography).
Results: The segmentation algorithm generated slabs used for OCT angiography *en face* visualization. We obtained Inner Retinal (ILM to OPL), Outer Retinal (OPL to RPE, OPL to BM, RPE to BM), Choriocapillaris, and Choroidal slabs. Expert comparison with OCT angiography images obtained with a supervised semi-automated segmentation showed equivalent results. Total processing time was below 30s in a Matlab environment on a Dell Precision laptop.
Conclusions: The algorithm produced a robust, fast segmentation on datasets from patients with a wide variety of retinal pathologies. It is shown to be useful for generating widefield OCT angiography slabs in a typical clinical setting.
Commercial Relationships: Giovanni Gregori, Carl Zeiss Meditec (P), Carl Zeiss Meditec (F); **Philip J. Rosenfeld**; **Luiz Roisman**, None; **Karen B. Schaal**, None
Support: Research support from Carl Zeiss Meditec. NIH Center Core Grant P30EY014801, DOD Grant# W81XWH-13-1-0048, Research to Prevent Blindness Unrestricted Grant, NIH Grant EY021834

Program Number: 447 **Poster Board Number:** A0084
Presentation Time: 1:30 PM–3:15 PM
Automated Ischemia Segmentation using OCT Angiography in Diabetic Retinopathy
Emily Cole[1, 2], Sabin Dang[1], Eduardo A. Novais[1, 3], Ricardo Louzada[1, 4], Caroline R. Baumal[1], Andre J. Witkin[1], Nadia K. Waheed[1], Jay S. Duker[1], Elias Reichel[1]. [1]Ophthalmology, Tufts University School of Medicine, Boston, MA; [2]Department of Electrical Engineering and Computer Science and Research Laboratory of Electronics, Massachusetts Institution of Technology, Boston, MA; [3]Federal University of São Paulo, São Paulo, Brazil; [4]Federal University of Goiás, Goiânia, Brazil.
Purpose: To evaluate whether an automated ischemia segmentation algorithm for optical coherence tomography angiography (OCTA) can identify disease severity of retinopathy in patients with diabetes.
Methods: Seventy-eight eyes from 40 patients with diabetes imaged on the RTVue XR Avanti AngioVue® platform were selected for image analysis. The dataset was chosen from consecutively imaged diabetic patients at New England Eye Center. No images were excluded for poor quality scans or motion artifact. We developed an algorithm which quantified geographic patches of non-perfusion on OCTA. This algorithm was able to identify poor quality scans and scale internal parameters to optimize signal to noise, thus no scans were excluded due to poor scan quality. The patients were stratified into five groups: diabetes without clinical diabetic retinopathy, mild/moderate/severe nonproliferative diabetic retinopathy (NPDR), and proliferative diabetic diabetic retinopathy (PDR). For each eye, the algorithm provided an OCTA ischemia index (OII) at the level of the superficial plexus, deep plexus, and choriocapillaris. An automated measurement of the FAZ was made at the level of the superficial and deep plexus. A chart review was performed to determine previous treatments (focal laser, PRP, anti-VEGF) as well as presence or absence of diabetic macular edema.
Results: The OII was validated with repeated measurements over 4 days from 10 normal eyes. The OII of the superficial plexus increases with worsening diabetic retinopathy severity, but this trend was not seen in the deep plexus or choriocapillaris. Figure 1 shows pairwise comparisons between the OII of the superficial plexus in each group, even when controlling for treatment. In the superficial plexus, there was a significant difference in the OII ($p<.05$) between diabetics without retinopathy and mild NPDR compared to all other groups. In the deep plexus, there was a significant difference in the OII between diabetics without retinopathy compared to those with retinopathy. Automated measurement of the FAZ showed a significantly larger FAZ in PDR compared to the other groups.
Conclusions: Automated algorithms can be used to assess the degree of ischemia in OCTA images from patients with diabetic retinopathy and may discriminate between different levels of disease

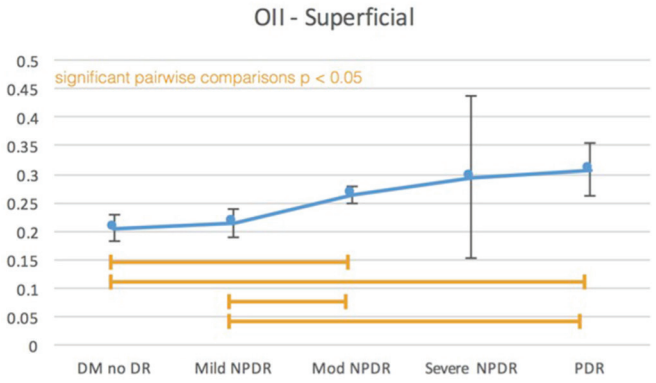

Commercial Relationships: Emily Cole, None; **Sabin Dang**, Patent Pending (P); **Eduardo A. Novais**, None; **Ricardo Louzada**, None; **Caroline R. Baumal**, None; **Andre J. Witkin**, None; **Nadia K. Waheed**, Patent Pending (P); **Jay S. Duker**; **Elias Reichel**, Patent Pending (P)

Program Number: 448 **Poster Board Number:** A0085
Presentation Time: 1:30 PM–3:15 PM
Artifact Removal and 3D Visualization for OCT Angiography
Brian Soetikno[1, 2], Justin Park[1], Hao F. Zhang[2], Amani A. Fawzi[1]. [1]Ophthalmology, Northwestern University, Chicago, IL; [2]Biomedical Engineering, Northwestern University, Evanston, IL.
Purpose: Optical coherence tomography angiography (OCTA) is an exciting, maturing imaging technology which may provide valuable information for assessing retinal disease. However, OCT angiograms have shadowing artifacts, making the visualization of the data challenging. Our goal was to explore a software workflow to visualize the three-dimensional (3D) architecture of inner retinal vessels from OCT angiography in both two-dimensional (2D) *en face* and 3D display formats.
Methods: We used the RTVue XR Avanti Optical Coherence Tomography Angiography (OCTA) instrument (Optovue Inc, Fremont, California, USA) to obtain 3D angiograms from healthy volunteers. The angiograms were exported from the OCTA device, enabling us to explore artifact removal and 2D/3D visualization techniques. For 2D *en face* display, we developed a simple method to produce composite images of the superficial and deep plexuses of the inner retinal network. Maximum amplitude projections (MAP) of the two plexuses were exported from the Optovue software. We then produced composite images in two steps: subtraction and color

merging, which were performed in MATLAB (R2015b, MathWorks) and Fiji (National Institutes of Health, Bethesda, MD, USA), respectively. For 3D display, we exported the angiography data and performed 3D layer segmentation to separate the superficial and deep plexus. We then converted the data into a standard 3D medical image format, which could then be loaded into various software packages for 3D visualization, including the MRIcroGL software package.
Results: Figure A shows a 2D MAP of the superficial plexus in a healthy control, and Figure B shows an example of a 2D MAP deeper plexus in the same patient. Figure C shows the final result of the deeper plexus after the subtraction process. We compared color composite images before and after subtraction as shown in Figure D and Figure E, respectively. The contrast between the superficial and deep plexi in Figure E is higher. Figure F shows an example of 3D display of the two plexuses (from a different patient) after our software pipeline.
Conclusions: We have successfully explored several methods for the visualization of OCTA data from the Optovue system, which will be useful in the future for better communication of the data among clinicians and scientists.

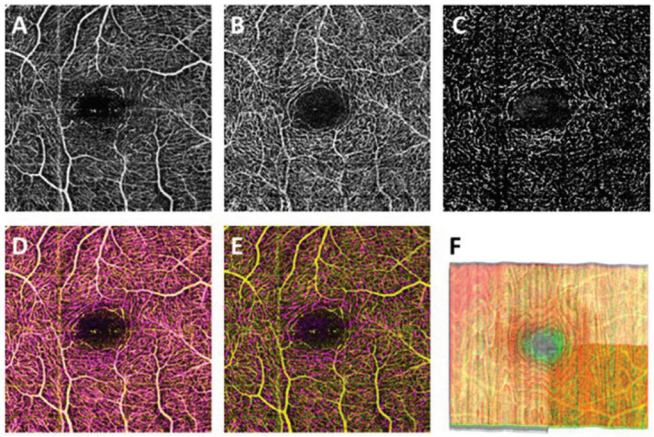

Commercial Relationships: Brian Soetikno, None; **Justin Park**, None; **Hao F. Zhang**, None; **Amani A. Fawzi**, None
Support: NIH 1DP3K108248-01, NIH R01EY019951-05

Program Number: 449 **Poster Board Number:** A0086
Presentation Time: 1:30 PM–3:15 PM
A novel approach to reducing decorrelation tail artifacts in OCT angiography
Homayoun Bagherinia[1], Jesse J. Jung[2], Soraya Rofagha[2], Patty Chung[2], Scott Lee[2], Michael Chen[1]. [1]Carl Zeiss Meditec, Inc., Dublin, CA; [2]East Bay Retina Consultants, Inc., Oakland, CA.
Purpose: To describe a mathematical approach to reducing decorrelation artifacts in OCT angiography (OCTA) images.
Methods: OCTA is prone to decorrelation tail artifacts due to the high scattering property of blood within overlying patent vessels, creating artifacts that interfere with the interpretation of OCTA images. We present a new approach for reducing the decorrelation tail artifacts based on an inverse problem estimation using two slab images generated from two or more retinal layers. A slab image of p=m×n can be generated by integrating, or other techniques to select a representative value of the cube motion contrast data within one or more layers. In the inverse problem approach discussed here, it is assumed that a lower slab image is generated as a result of mixture of an upper slab (a sub-volume above the lower layer) and the lower slab image without decorrelation tail artifacts (the unknown image to reconstruct). Assuming a multiplicative mixing model, an inverse formulation of decorrelation tail problem is $\min_x \|WAx-b\|^2+\alpha\|\Gamma x\|^2$, where A is a diagonal p×p matrix whose diagonal elements are the pixel values of the upper slab image, W is a diagonal p×p matrix containing the weight values for each pixel of the upper slab image, b is a column vector of p whose elements are the pixel values of the lower slab image, α is the regularization parameter, Γ is a matrix of p×p which contains filters that enforce smoothness. x is a column vector of p whose elements are the pixel values of the lower slab image with reduced decorrelation tail artifacts.
Results: The figures below show examples of decorrelation artifacts reduction by our method for macular telangiectasia (Mac Tel) type 2, and subretinal neovascular membrane (SRNVM) cases before and after reducing the decorrelation artifacts using CIRRUS (ZEISS Dublin, CA).
Conclusions: We have presented a mathematical approach to reduce the inner and outer retinal decorrelation tail artifacts in OCTA images. Our approach can be utilized for visualization and interpretation of various disease cases such as SRNVM and Mac Tel.

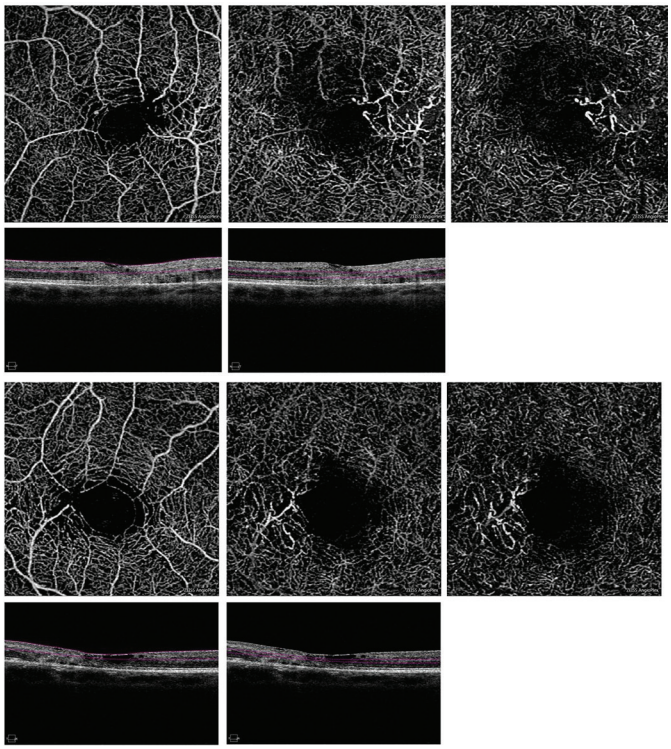

Mac Tel type 2 examples from left to right: superficial capillary plexus, deep capillary plexus (DCP) with corresponding B-scans; and DCP with reduced decorrelation artifacts.

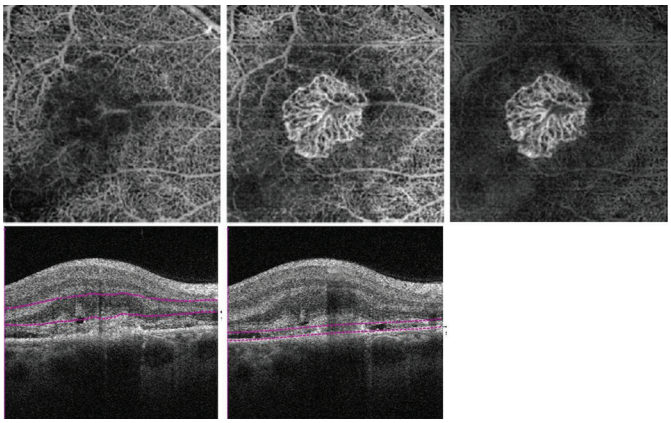

SRNVM case from left to right: DCP and custom slab segmenting the type 2 neovascular membrane with corresponding B-scabs; and the custom slab with reduced decorrelation artifacts.

Commercial Relationships: Homayoun Bagherinia, Carl Zeiss Meditec, Inc; **Jesse J. Jung**, Carl Zeiss Meditec, Inc (C); **Soraya Rofagha**, Carl Zeiss Meditec, Inc (C); **Patty Chung**, Carl Zeiss Meditec, Inc (C); **Scott Lee**, Carl Zeiss Meditec, Inc (C); **Michael Chen**, Carl Zeiss Meditec, Inc (C)

Program Number: 450 **Poster Board Number:** A0087
Presentation Time: 1:30 PM–3:15 PM

Projection-Resolved Optical Coherence Tomographic Angiography

Zhang Miao, Thomas S. Hwang, J. Peter Campbell, Steven T. Bailey, David J. Wilson, David Huang, Yali Jia. Casey Eye Institute, Oregon Health and Science University, Portland, OR.

Purpose: To describe a novel method to remove shadowgraphic projection artifacts in optical coherence tomography angiography (OCT-A)

Methods: 3x3 mm OCT-A were obtained with a 70 kHz commercial OCT (RTVue-XR) and the split-spectrum amplitude-decorrelation angiography (SSADA) algorithm. A novel projection-resolved (PR) resolves the ambiguity between in-situ flow and projected flow by comparing the decorrelation value of each voxel to all shallower voxels within the same axial scan. Slab subtraction (SS), a common method to suppress projection, is used for comparison.

Results: One eye each of 13 healthy human participants (age 25 to 58 years) were scanned in the macula. The average PR results in the parafoveal region show 3 peaks of vessel density that corresponds to the superficial (nerve fiber and ganglion cell layers), intermediate (between inner plexiform and inner nuclear layers [INL]), and deep (between INL and outer plexiform layer [OPL]) plexuses. These vessel density peaks could not be identified on the OCT angiogram without projection suppression or with SS suppression. In OCT-A without projection suppression, deeper slabs are dominated by projection artifacts from the superficial slab. SS suppression removed most projection artifacts from the deeper slabs, but fragmented the capillary network in the intermediate and deep plexuses. PR OCT-A successfully removed projection artifacts while preserving vascular network continuity in the deeper plexuses. PR OCT-A is the only algorithm able to produce truly depth-resolved cross-sectional angiograms with discrete vessels without long tails.

Conclusions: PR OCT-A effectively suppresses the projection artifact while preserving vascular detail in deeper layers. This novel technique is able to, for the first time, resolve 3 distinct retinal vascular plexuses of the human eye non-invasively *in vivo*. The location of the 3 plexuses agree with previous histology results.

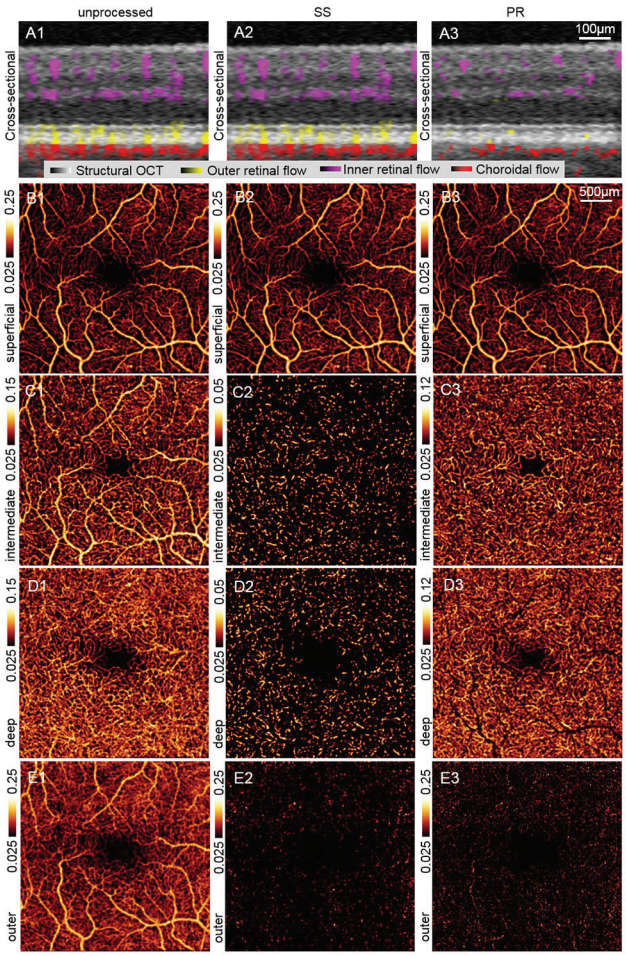

Fig. 1. Cross-sectional angiograms (Row A) and *en face* superficial plexus (Row B), intermediate plexus (Row C), deep plexus (Row D), and outer retinal slab (Row E) angiograms of unprocessed (Column 1), slab-subtracted (SS, Column 2), and projection-resolved (PR, Column 3) OCT-A.

Commercial Relationships: Zhang Miao, None; **Thomas S. Hwang**, None; **J. Peter Campbell**, None; **Steven T. Bailey**, None; **David J. Wilson**, None; **David Huang**, Optovue, Inc (I), Optovue, Inc (R), Optovue, Inc (P), Optovue, Inc (F), Carl Zeiss Meditec, Inc (P); **Yali Jia**, Optovue, Inc (F), Optovue, Inc (P)

Support: NIH grants R01 EY024544, DP3 DK104397, R01 EY023285, P30 EY010572 and an unrestricted grant from Research to Prevent Blindness.

Program Number: 451 **Poster Board Number:** A0088
Presentation Time: 1:30 PM–3:15 PM

Sensitivity enhancement of intrinsic optical signal recording through split-spectrum-optical coherence tomography

Damber Thapa[1], Benquan Wang[1], Yiming Lu[1], Taeyoon Son[1], Xincheng Yao[1, 2]. [1]Department of Bioengineering, University of Illinois at Chicago, Chicago, IL; [2]Department of Ophthalmology and Visual Sciences, University of Illinois at Chicago, Chicago, IL.

Purpose: Intrinsic optical signal (IOS) imaging that measures transient light changes correlated with retinal physiological activation promises to be a new methodology for high resolution mapping of

retinal neural dysfunctions. However, its practical applications for noninvasive examination of retinal function have been hindered by low signal-to-noise ratio (SNR) and small magnitude of IOSs. Split-spectrum amplitude-decorrelation has been demonstrated to improve image quality of optical coherence tomography (OCT) angiography. The purpose of this study is to test if the split-spectrum strategy can be used to enhance the sensitivity of IOS recording.
Methods: Freshly enucleated leopard frog (Rana Pipiens) eyes were used in this study. A spectral domain OCT (SD-OCT) that uses a broadband superluminescent diode (D-840-HP-I, Superlum, Ireland) with a center wavelength of 845.8 nm, full width at half maximum (FWHM, Δλ) of 100 nm, was constructed for functional OCT imaging of retinal IOSs. The full spectrum of SD-OCT was divided into three overlapping spectral bands: first band includes data in the wavelength range 780-850 nm, second band in the wavelength range 815-885 nm and third band in the wavelength range 850-920 nm. The splitted bands were zero padded to match the length of the full spectrum. Three IOS images were calculated separately from individual spectral band OCT first, and were merged into a single frame using a maximum projection method.
Results: IOSs were calculated at the photoreceptor layer of the SD-OCT images. The proposed method considerably increased the IOS detection compared to the full spectrum method. The active pixel number (pixels that produce IOS) increased by at least two-fold and they were significantly greater ($p>0.01$) than those of the full spectrum. The peak amplitude amplified by at least twice using split-spectrum method compared to the full spectrum.
Conclusions: The experimental results show that IOS sensitivity can be improved by amalgamating IOSs from split-spectrum OCTs. The split-spectrum technique reduces the correlation between the spectral bands; therefore, the IOSs which are lost in one spectral band can be acquired from other spectral bands. The proposed method resolves some of the challenges encountered by IOS imaging to increase signal amplitude and SNR, which is essential for practical applications of functional IOS imaging.
Commercial Relationships: Damber Thapa; **Benquan Wang**, None; **Yiming Lu**, None; **Taeyoon Son**, None; **Xincheng Yao**, The UAB RESEARCH FOUNDATION (P)
Support: NIH R01 EY023522, NIH R01 EY024628, NIH P30 EY001792 and NSF CBET-1055889

Program Number: 452 **Poster Board Number:** A0089
Presentation Time: 1:30 PM–3:15 PM
Swept source OCT angiography based on ratio analysis
Charles A. Reisman, Zhenguo Wang, Jonathan J. Liu, Qi Yang, Ying Dong, Kinpui Chan. Topcon Advanced Biomedical Imaging Laboratory, Topcon Medical Systems, Oakland, NJ.
Purpose: To demonstrate an innovative OCT angiography method with improved detection sensitivity of low blood flow and reduced motion artifacts without compromising axial resolution using commercially available swept source OCT (SS-OCT).
Methods: We performed SS-OCT imaging (DRI OCT-1, Topcon, Tokyo, Japan) at 100,000 A-scans per second in both healthy and diseased eyes. Volumetric OCT scans were acquired with real-time tracking using infrared fundus images. OCT angiography scans were typically acquired over a 3mm x 3mm field of view on the retina and consisted of up to 320 A-scans x 320 B-scan positions where each B-scan position was repeatedly scanned 4 times.
For SS-OCT angiography processing, our newly developed OCT Angiography Ratio Analysis (OCTARA) was performed. B-scan repetitions at each scan location were registered. The one-sided ratio analysis was computed between corresponding image pixels as defined in Fig. 1, where $I(x, y)$ is the OCT signal intensity, N is the number of scanned B-scan combinations at the given location, and i and j represent the two frames within any given combination of frames. Motion artifacts were suppressed by active tracking during scan acquisition and by selectively averaging over multiple B-scan combinations.
Results: The ratio analysis is a relative measurement of OCT signal amplitude change and enhances the minimum detectable signal compared to other techniques based on variance and decorrelation measurements. Our OCTARA method preserves the integrity of the entire spectrum and therefore does not suffer from compromised axial resolution, an inherent disadvantage of split-spectrum OCT angiography techniques. Using OCTARA, vascular structure is more uniformly visualized with better detection sensitivity of low flow compared to intensity differentiation-based optical microangiography (OMAG). The vascular network is also better visualized compared to split-spectrum amplitude-decorrelation angiography (SSADA) where differences in relative angiographic signal intensity are due both to the separate factors of full-spectrum versus split-spectrum and of ratio versus amplitude decorrelation calculations.
Conclusions: Our innovative OCT angiography processing method, based on a ratio calculation, demonstrates improved detection sensitivity of microvasculature while preserving axial resolution.

$$r(x,y) = 1 - \frac{1}{N}\sum_{i,j}^{N}\frac{\min(I_i(x,y), I_j(x,y))}{\max(I_i(x,y), I_j(x,y))}$$

Figure 1: Ratio Analysis Calculation
Commercial Relationships: Charles A. Reisman, Topcon Medical Systems; **Zhenguo Wang**, Topcon Medical Systems; **Jonathan J. Liu**, Topcon Medical Systems; **Qi Yang**, Topcon Medical Systems; **Ying Dong**, Topcon Medical Systems; **Kinpui Chan**, Topcon Medical Systems

Program Number: 453 **Poster Board Number:** A0090
Presentation Time: 1:30 PM–3:15 PM
Contrast-enhanced OCT angiography of the choriocapillaris
Vivek J. Srinivasan[1, 2], Conrad Merkle[1], Marcel Bernucci[1], Conor Leahy[1]. [1]Biomedical Engineering, UC Davis, Davis, CA; [2]Ophthalmology, UC Davis, Sacramento, CA.
Purpose: Though Optical Coherence Tomography (OCT) angiography can clearly image the choriocapillaris in cases of Retinal Pigment Epithelium (RPE) atrophy, methods that assess the choriocapillaris beneath an intact RPE are lacking. To address these limitations, we use Intralipid-20% (FDA-approved for intravenous parenteral nutrition in humans) as a contrast agent to fill under-perfused vessels and enhance scattering signal in vessels beneath an intact RPE. By combining contrast enhancement with a long imaging wavelength and a customized image processing technique for further vessel enhancement, we image the choriocapillaris in the rat retina with a level of detail approaching that of histology.
Methods: A 1300 nm spectral / Fourier domain OCT ophthalmoscope was adapted for imaging the rat retina at a speed of 92,000 axial scans per second. The axial and transverse resolutions were approximately 7 microns in air. Sprague-Dawley rats (n = 3) were anesthetized with isoflurane. Imaging was performed both before and after intravenous injection of Intralipid-20% (used here as a contrast agent). The total injected volume was ~2.5% of the total blood volume. A Hessian-based algorithm was used for scale-dependent enhancement vessels in the angiograms.
Results: Pre-contrast OCT angiograms clearly show the microvascular networks throughout the retina (A), as well as large

vessels in the choroid (B, depth is color-coded). Post-contrast OCT angiograms better accentuate the retinal capillaries (C), and particularly, highlight microvasculature in the choriocapillaris that was not previously visualized (D, depth is color-coded).
Conclusions: Here we demonstrate the value of exogenous contrast enhancement for OCT angiography of microvasculature, particularly in the choriocapillaris. While the results show that contrast enhancement provides a clear benefit in imaging Sprague-Dawley rats, future work is required to test the benefits in more highly pigmented eyes. These methods will improve the monitoring of early age-related macular degeneration in experimental models, and potentially also in human subjects.

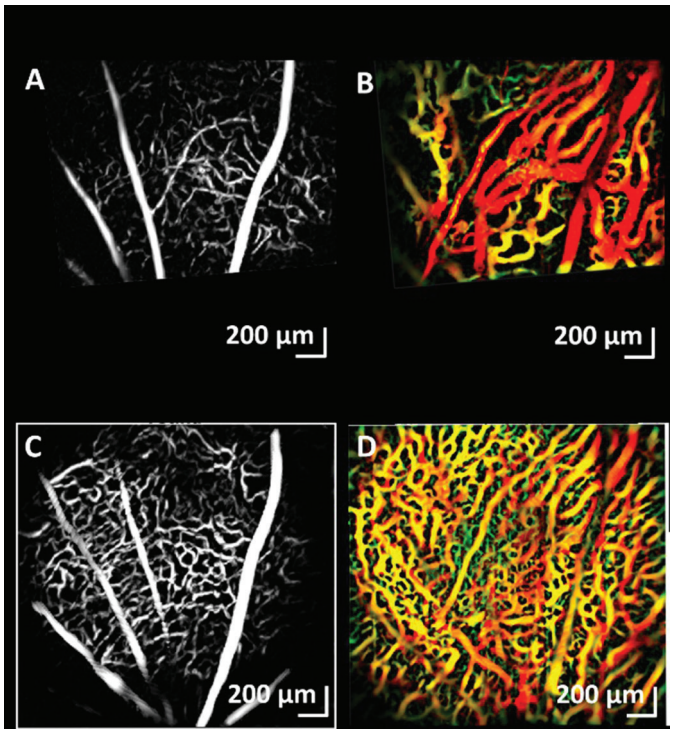

Retinal (A) and choroidal (B) maximum intensity projection (MIP) angiograms without contrast agent. Only the large choroidal vessels are visible in B). Retinal (C) and choroidal (D) MIP angiograms after injection of 2 mL kg^{-1} of the contrast agent, Intralipid-20%. The choriocapillaris is more prominent in post-contrast angiogram.
Commercial Relationships: Vivek J. Srinivasan, Optovue, Inc. (P); **Conrad Merkle**; **Marcel Bernucci**, None; **Conor Leahy**, Carl Zeiss Meditec, Ltd.
Support: Glaucoma Research Foundation

Program Number: 454 **Poster Board Number:** A0091
Presentation Time: 1:30 PM–3:15 PM
OCT retinal angiography using neural networks
Maciej Szkulmowski[1], Daniel Ruminski[1], Pawel Liskowski[2], Bartosz Wieloch[2], Krzysztof Krawiec[2], Bartosz Sikorski[3, 4], Maciej D. Wojtkowski[1]. [1]Institute of Physics, Nicolaus Copernicus University, Torun, Poland; [2]Laboratory of Intelligent Decision Support Systems, Poznan University of Technology, Poznan, Poland; [3]Department of Ophthalmology, Nicolaus Copernicus University, Bydgoszcz, Poland; [4]Collegium Medicum, Nicolaus Copernicus University, Bydgoszcz, Poland.
Purpose: To demonstrate noninvasive visualization of retinal microcapillary network (RMN) in retinal diseases with deep convolutional neural network (CNN) using data from recently developed device combining Scanning Laser Ophthalmoscope (SLO) and Spectral Optical Coherence Tomography (SOCT). SLO system provides fast eye tracking system while SOCT delivers 3D data for knowledge-free vessel segmentation technique.
Methods: The study was performed with ultra high resolution and high speed SOCT laboratory setup (100,000 Ascans/sec, 4.5 um axial resolution, 91 dB detection sensitivity). Constant 30 Hz retinal preview is provided by the SLO device and is used to guide the SOCT scanning beam to the region of interest. To increase RMN visualization area mosaic protocols were used. In case of eye blink or data corruption SOCT guided by SLO can still provide good quality RMN maps as corrupted B-scans are rejected and reacquired. RMS maps are created from 3D SOCT data using supervised machine learning algorithm using deep convolutional neural network (CNN) trained on data acquired from a set of 10 eyes (from both healthy volunteers and patients with retinal diseases) with vessels labeled by three independent skilled specialists. Each labeled voxel with a small cube of neighboring voxels forms an example. Examples are split into disjoint training and test sets. The CNN consists of 7 layers and is trained by stochastic gradient descent with batch updates and momentum (equivalent to multinomial logistic regression).
Results: Trained CNNs provide sensitivity and specificity for RMN detection in training sets between 0.95 and 0.98 depending on training algorithm. We will show RMN maps obtained using CNNs with both proposed approach for 4 healthy volunteers and 12 patients with diabetic retinopathy, branch retinal vein occlusion and central retinal vein occlusion. We will compare the maps obtained using CNN with maps obtained using standard phase-variance angiographic algorithms.
Conclusions: Our results shows that CNN approach to RMN visualization provides accurate vessel detection incorporating a priori knowledge of skilled specialists and allows for increased sensitivity and specificity of SOCT based angiography.
Commercial Relationships: Maciej Szkulmowski, None; **Daniel Ruminski**, None; **Pawel Liskowski**, None; **Bartosz Wieloch**, None; **Krzysztof Krawiec**, None; **Bartosz Sikorski**, None; **Maciej D. Wojtkowski**, None
Support: National Center for Research and Development Grant No. PBS1/A9/20/2013

Program Number: 455 **Poster Board Number:** A0092
Presentation Time: 1:30 PM–3:15 PM
Speckle-noise free choroidal angiography and vessel surface area measurement with Spectral OCT
Peter Maloca. Ophthalmology OCTlab, University of Basel, Basel, Switzerland.
Purpose: Approximately 95% of the ocular blood flow is directed to the uveal system, of which approximately 70% is circulating into the choroidal vessels. We visualize these vessels and measure their surface with speckle-noise freed 3D optical coherence tomography.
Methods: 3DOCT volumes were obtained from 20 healthy eyes (10 females) with Spectralis OCT (Heidelberg Engineering, Heidelberg, Germany). The scan pattern was raster lines 4.5x3.0x1.9 mm, 261 B-Scans, with EDI-mode on, averaged for 20 scans using the automatic averaging and tracking tool. The OCT volumes were freed from speckle-noise with a prototype denoising analysis software. Choroidal vessels were segmented and their total surface area was calculated.
Results: 20 eyes of healthy females were investigated. The mean central choroidal vessel surface area was 0.18444301 mm2 (range 0.154483253 mm2 - 0.215696694 mm2; SD 0.01882505). Three dimensional models of the choroidal vessels were reconstructed.

Conclusions: Speckle-noise free chororoidal angiography and surface measurement may be a potential complementary 3D visualization technology for choroidal vessels.

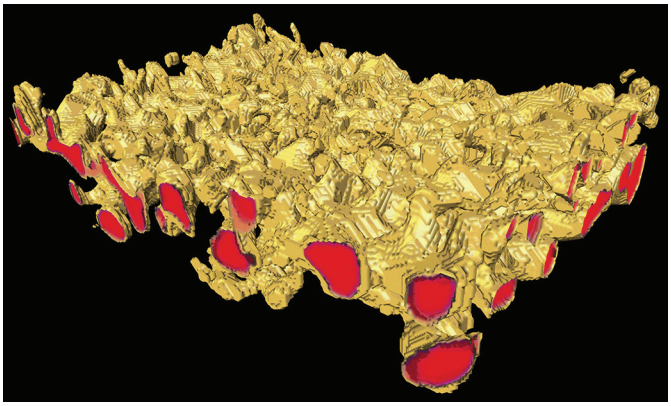

Speckle-noise free 3DOCT angiography of choroidal vessels.**Commercial Relationships: Peter Maloca**

Program Number: 456 **Poster Board Number:** A0093
Presentation Time: 1:30 PM–3:15 PM
Methods for Quantification of Image Quality in OCT Angiography Images
Carmen J. Yoo[1], Michael Chen[1], Mary K. Durbin[1], Zhongdi Chu[2], Ruikang K. Wang[2], Chieh-Li Chen[2], Jesse J. Jung[3], Scott Lee[3].
[1]Clinical & Applications Development, Carl Zeiss Meditec, Inc, Dublin, CA; [2]University of Washington, Seattle, WA; [3]East Bay Retina Consultants, Oakland, CA.
Purpose: OCT angiography (OCTA) image quality is an important factor when interpreting scans for assessment and diagnosis of retinal pathology. Our purpose is to determine the inter-grader repeatability for evaluating the quality of spectral-domain optical coherence tomography angiography (SD-OCTA) images and to correlate quantitative measures to subjective assessment.
Methods: Cirrus AngioPlex OCTA (Carl Zeiss Meditec, Dublin, CA) 3X3 images were acquired from 20 eyes of 20 subjects. Superficial retinal capillary plexus (slab) images were obtained of pathologies including wet age-related macular degeneration, retinal angiomatous proliferation, retinal arteriolar macroaneurysm, branch retinal vein occlusion, sickle-cell maculopathy, central serous retinopathy, and diabetic macular edema. Image selection purposely included sub-optimal images in order to have a broad range of quality; 75% of the images were well segmented. Image quality was graded by two optometrists, one with extensive experience in SD-OCTA analysis and another with limited experience, using a scale of 1=unusable, 2=poor quality, able to see some information, 3=fair, image quality affects ability to assess, 4=good, artifacts, if any, do not interfere with assessment, 5=excellent. Intra-class correlation (ICC) was used to determine inter-grader repeatability. In addition, four image quality metrics were calculated: connectivity of angiogram, angiogram contrast, angiogram signal to noise ration (aSNR) and the number of connected components (NCC). These were correlated to mean subjective grade. The range of the metrics in good scans of 15 normal eyes was also established.
Results: Mean and standard deviation (SD) values for the four metrics are shown in the table. Inter-grader qualitative reproducibility was good with an ICC of 0.76.
Conclusions: Image quality can be evaluated by trained graders with good repeatability. Overall, there is a poor correlation between qualitative and quantitative assessment, but an objective parameter that correlates well to subjective assessment is the NCC. This may be due to the emphasis of the qualitative criterion on pathology assessment and diagnosis.

Parameter	Range in good scans of Normal Eyes	Mean in Diseased Eyes(SD)	Correlation to Subjective Grade (R^2)	p-value for linear fit
Connectivity	4.8-6.1 *10^{-4}	7.2 (1.1) *10^{-4}	0.35	0.006
Contrast	2.4 – 3.0	2.1 (0.4)	0.42	0.002
aSNR	5.4 – 6.5	6.9 (1.0)	0.008	0.71
NCC	670 – 1200	1247 (620)	0.87	3 * 10^{-9}

Commercial Relationships: Carmen J. Yoo, Carl Zeiss Meditec, Inc.; **Michael Chen**, Carl Zeiss Meditec, Inc.; **Mary K. Durbin**, Carl Zeiss Meditec, Inc.; **Zhongdi Chu**, Carl Zeiss Meditec, Inc. (C); **Ruikang K. Wang**, Carl Zeiss Meditec, Inc. (C), Carl Zeiss Meditec, Inc. (R), Carl Zeiss Meditec, Inc. (P), Carl Zeiss Meditec, Inc. (F); **Chieh-Li Chen**, Carl Zeiss Meditec, Inc. (C); **Jesse J. Jung**, Carl Zeiss Meditec, Inc. (C); **Scott Lee**, Carl Zeiss Meditec, Inc. (C)

Program Number: 457 **Poster Board Number:** A0094
Presentation Time: 1:30 PM–3:15 PM
OCT Angiography Volume Image Compression
Milton Wei. Carl Zeiss Meditec, Dublin, CA.
Purpose: Oct angiography scans contain phase information as well as intensity information. The purpose is to reach maximum compression for both phase and intensity volume images without losing any pathology information contained in the original angiography OCT scans.
Methods: Different image compression formats including JPEG, JPEG-LS, PNG etc. were used to compress intensity volume and phase volume of OCT angiography scans of eye patients. A variety of compression rate from 5% to 50% were used for each compression format. Segmentation results of processed intensity volumes (recovered or uncompressed from compressed images) and original intensity volumes were compared to make sure that ILM, RPE etc. layers were still correctly segmented. Enface or slab calculation of phase volume were used to judge if any pathology information was lost during compression. Since enface calculation was also based on the segmentation results of intensity volume, to make thing simple, only the segmentation results of original volume were used. And then slabs calculated from the processed phase volume images for each level of compression rate were compared to the results calculated from original phase volumes. Compression time was also recorded and was considered as another factor. However due to the improvement of compression tools and computer speed, the compression performance was not as critical as the quality.
Results: Some types of compression on intensity volume showed artifacts which had impact on segmentation results. The situation became worse when higher compression rates were used for these type of compression formats. So they were not suitable as compression methods for OCT intensity volume images. However, phase volumes compressed by different kind of compression format and rate did not show significant differences on enface or slab results. So we had big freedom to choose compression method and rate on phase volumes.

Conclusions: The compression format and maximum compression rate without losing any important pathology information were decided for both intensity and phase volume of OCT angiography scans.

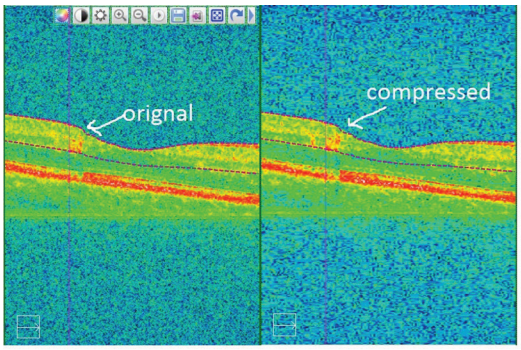

Segmentation results comparison - one from compressed intensity volume, the other is from orignal volume

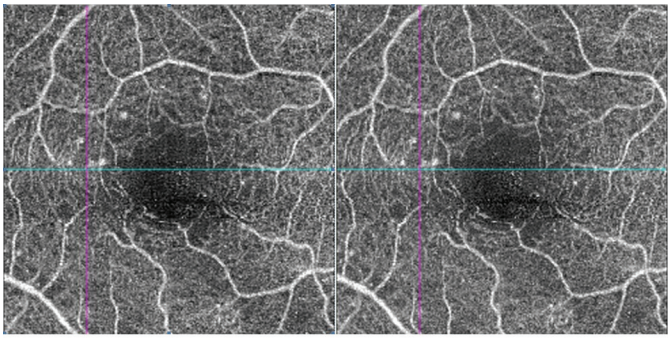

Slabs calcated form compressed phase volume and from orignal phase volume**Commercial Relationships: Milton Wei**

Program Number: 458 **Poster Board Number:** A0095
Presentation Time: 1:30 PM–3:15 PM
Level-Set Algorithm to Improve the Reliability of Vessel Density and Avascular Area Measurements in Optical Coherence Tomography Angiography
Audra Miller[1], Changlei Dongye[1, 2], Thomas S. Hwang[1], Yali Jia[1].
[1]Casey Eye Institute, Oregon Health & Science University, Portland, OR; [2]College of Information Science and Engineering, Shandong University of Science and Technology, Qingdao, China.
Purpose: To improve the repeatability and reproducibility measurements of vessel density and avascular area in optical coherence tomography (OCT) angiography
Methods: 3x3 mm macular scans of healthy eyes were taken using a spectral OCT system (RTVue-XR, Optovue, Inc.). The Split-Spectrum Amplitude Decorrelation Angiography (SSADA) algorithm produced an *en face* inner retinal angiogram by segmenting anterior to the outer boundary of inner plexiform layer. An algorithm using the fuzzy C-means method detected vasculature with high decorrelation values. The level-set method refined the separation between vessels and noise artifacts. Then, the extracted vessel binary maps were processed to measure: 1. Vessel area density (VAD): percentage area occupied by vasculature in the selected area, 2. Vessel length density (VLD): length of skeletonized vasculature divided by the area and 3. Avascular area: area of decorrelation values detected below the threshold derived by a function of level set evolution. The intra-visit repeatability and inter-visit reproducibility were calculated in terms of coefficient of variation (CV). The reliability was compared to prior work that used a fixed cutoff to extract vessels and the commercial software (AngioAnalytics) available on RTVue-XR.
Results: The scans from 32 healthy adults with a signal strength index (SSI) >60 were included. The mean VAD varied in different algorithms. The level-set method measured VAD and FAZ with greater repeatability and reproducibility compared to the other methods. The new parameter VLD was similarly reliable. The FAZ was automatically detected and quantified in subjects with a wide range of SSI, indicating less dependency on signal strength (Fig 1).
Conclusions: Level-set algorithm for quantification of vessel density and avascular areas in OCT angiography is more reliable compared to fixed cutoffs or currently available commercial software. Further testing in diseased eyes can validate its clinical utility.

	Level-Set			Fixed-Threshold		AngioAnalytics
	VAD	VLD	FAZ	VAD	FAZ	VAD
Mean ± SD (N=22)	75.0 ±3.7	30.7 ±1.8	0.22 ±0.1	88.3 ±11.2	0.36 ±0.39	52.6 ±3.1
Repeatability (N=22)	1.5%	2.8%	6.5%	2.3%	11.4%	2.2%
Reproducibility (N=5)	1.0%	5%	5.17%	3.9%	16.1%	1.5%

Vessel Area Density (VAD, unit= % area); Vessel Length Density (VLD, unit= 1/mm)

Table 1. Level-Set vs. Fixed-Threshold vs. AngioAnalytics

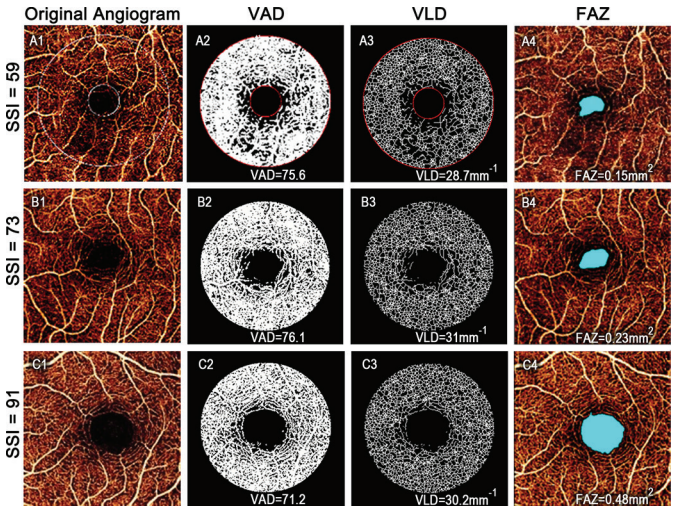

Figure 1. OCT angiograms of normal subjects with varied signal strength index (SSI) were analyzed for vessel area density (VAD) and vessel length density (VLD) of the perifovea (0.3-1.25 mm from foveal center). Automatically detected FAZ is displayed in blue.
Commercial Relationships: Audra Miller, None; **Changlei Dongye**, None; **Thomas S. Hwang**, None; **Yali Jia**, Optovue, Inc. (P), Optovue, Inc. (F)
Support: NIH Grants DP3 DK104397, R01 EY024544, R01 EY023285, P30-EY010572, and an unrestricted grant from Research to Prevent Blindness

Program Number: 459 **Poster Board Number:** A0096
Presentation Time: 1:30 PM–3:15 PM
Automated Quantitative Analysis of the Fovea using OCT Angiography
Morgan Heisler[1], Pavle Prentasic[2], Sieun Lee[1], Zaid Mammo[3], Ahmad Ibrahim[1], Andrew Merkur[3], Eduardo Navajas[3], Mirza Faisal Beg[1], Sven Loncaric[2], Marinko V. Sarunic[1]. [1]School of Engineering Science, Simon Fraser University, Burnaby, BC, Canada; [2]Faculty of Electrical Engineering and Computing, University of Zagreb, Zagreb, Croatia; [3]Department of Ophthalmology and Visual Sciences, University of British Columbia, Vancouver, BC, Canada.

Purpose: To present an automated pipeline for quantitative analysis of the foveal vasculature and Foveal Avascular Zone (FAZ) acquired with Optical Coherence Tomography Angiography (OCTA).
Methods: Twelve eyes from six normal human subjects were imaged with a 1060-nm, 100-kHz custom-built OCTA system. Automated techniques were used to quantify the FAZ metrics (area, greatest diameter, and lowest diameter) and capillary density surrounding the FAZ. Deep convolutional neural networks were used for automated segmentation of the retinal microvasculature in order to calculate the capillary density.
Results: The morphometry of the FAZ and perifoveal capillaries determined by the automated tools were compared with the results from a human rater. The minimum diameter (manual: 501µm ± 72µm, automated: 482µm ± 75µm), maximum diameter (manual: 734µm ± 103µm, automated: 733µm ± 116µm) and area (manual: 0.308mm2 ± 0.074mm2, automated: 0.294mm2 ± 0.071mm2) were calculated. The accuracy of the automated blood vessel segmentation was evaluated by pixel-wise comparison of the manually segmented image with the thresholded output of the neural network. Using this method, blood vessel segmentation reached a mean accuracy of ~81%.
Conclusions: The methods used here for automated quantitative analysis of OCT Angiography were shown to be accurate when compared to a manual rater. Further work is required is validate the utility of these methods in creating an automated retinal vascular disease screening system.

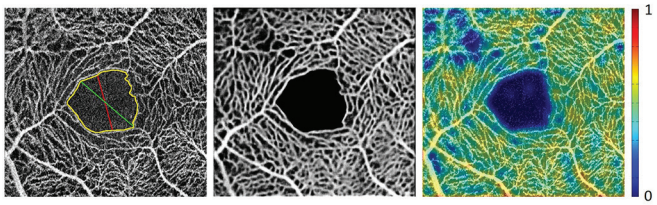

Left: Automated results of the minimum (red) and maximum (green) FAZ diameter and perimeter (yellow). Middle: Automated vessel segmentation results. Right: Capillary perfusion map.
Commercial Relationships: Morgan Heisler, None; **Pavle Prentasic**, None; **Sieun Lee**, None; **Zaid Mammo**, None; **Ahmad Ibrahim**, None; **Andrew Merkur**, None; **Eduardo Navajas**; **Mirza Faisal Beg**, None; **Sven Loncaric**, None; **Marinko V. Sarunic**, None
Support: Brain Canada, National Sciences and Engineering Research Council of Canada, Canadian Institutes of Health Research, Alzheimer Society Canada, Pacific Alzheimer Research Foundation, Michael Smith Foundation for Health Research, Genome British Columbia

Program Number: 460 **Poster Board Number:** A0097
Presentation Time: 1:30 PM–3:15 PM
Reproducibility of Foveal Avascular Zone measurements across four different Optical Coherence Tomography Angiography systems
Mariano Cozzi, Stefano Erba, Alessandro Invernizzi, Marco Pellegrini, Giovanni Staurenghi. Biomedical and clinical sciences, Eye Clinic Luigi Sacco Hospital, University of Milan, Milan, Italy.
Purpose: Foveal avascular zone (FAZ) has been assessed by different authors using Optical Coherence Tomography Angiography (OCTA) in healthy and pathologic eyes. The aim of our study is to investigate the reproducibility of FAZ area in healthy subjects on four different Spectral Domain OCTA and calculate inter observer agreement.
Methods: This is a cross-sectional non-interventional study. A 3mm x 3mm scan pattern of the right eye was obtained for each instrument. Subjects were scanned on AngioVue (Optovue RTVue XR Avanti, Optovue Inc.) based on a split spectrum amplitude decorrelation angiography (SSADA) algorithm; Zeiss AngioPlex (Cirrus HD-OCT 5000, Carl Zeiss Meditec Inc.) based on a so called optical micro-angiography complex (OMAG) modality; a prototype Spectralis OCT2 module (Heidelberg Spectralis, Heidelberg Engineering) based on a full spectrum amplitude decorrelation algorithm; and a prototype of AngioScan (RS-3000 Advance OCT, Nidek Co., Ltd) based on a so called complex decorrelation algorithm, processing both phase and amplitude of the signal.
Superficial vascular plexus was segmented using inbuilt semi automatic softwares present on each instrument. En face OCT slabs were segmented with an inner boundary at 3 microns beneath internal limiting membrane (ILM) and an outer boundary set at 15 microns beneath inner plexiform layer (IPL).
After exporting images, two masked graders reviewed and calculated manually FAZ area using ImageJ (ImageJ 1.49v; National Institutes of Health), a publicly available image processing software.
Interclass correlation coefficient (ICC) was calculated between graders and instruments.
Results: 15 eyes of 15 subjects (mean age 27,6 SD±4,7 years) were scanned by two different operators. All images had good quality with gradable FAZ at the superficial vascular plexus.
The mean FAZ area was 0,23 mm^2 SD ± 0,08 for AngioVue, 0,24 mm^2 SD±0,08 for OCT2 and AngioPlex and 0,25 mm^2 SD±0,09 for AngioScan.
Inter observer agreement was excellent for all the instruments, ICC>0,98. Agreement between 4 technologists was high ICC=0,94.
Conclusions: Our results provide a significant reproducibility of FAZ measurements in healthy subjects using four different OCTA technologists. As reported in previous publications inter observer reproducibility was high using ImageJ software. Dedicated automatic softwares would be a useful implement for quantitative analysis.
Commercial Relationships: Mariano Cozzi, Bayer AG (F), Heidelberg Engeneering (F), Alcon (F); **Stefano Erba**, None; **Alessandro Invernizzi**, None; **Marco Pellegrini**, None; **Giovanni Staurenghi**, Heidelberg Engeneering (C), Quantel Medical (F), Quantel Medical (C), GSK (C), Heidelberg Engeneering (F), Bayer AG (F), OD-OS (C), Genentech (C), Carl Zeiss Meditec (C), Ocular instruments (P), Allergan (C), Boheringer (C), Bayer AG (C), Allergan (F), Roche (C), Novartis (C), QLT (C), Alcon (C), Alcon (F), Optos (C)

Program Number: 461 **Poster Board Number:** A0098
Presentation Time: 1:30 PM–3:15 PM
Measurement of pulsatile retinal blood flow in normal human eyes using Doppler Fourier-domain optical coherence tomography
Meixiao Shen, Shenghai Huang, Ce Shi, Fan Lu. School of Ophthalmology & Optometry, Wenzhou Medical University, Wenzhou, China.
Purpose: To measure pulsatile retinal blood flow in normal human eyes using Doppler Fourier-domain optical coherence tomography (FD-OCT).
Methods: Ten normal people aged 25 to 40 years were measured for the left eye at optic nerve heads using Doppler FD-OCT. An improved phase-resolved algorithm was used to obtain the Doppler shift by calculating phase differences between sequential A-scans. Four indices, including pulsatility index (PI), resistance index(RI), peak systolic velocity (S) / average velocity (A) ratio, end distalic velocity (D)/A ratio were calculated to quantify the pulsatile retinal

blood flow based on the Doppler spectrum of the flow. The left eye of each subject was imaged two times by the first examiner to assess intra-observer repeatability and once by the second examiner to assess inter-observer reproducibility. The intraclass correlation coefficient (ICC) and coefficients of repeatability and reproducibility (COR) were analyzed to evaluate the reliability.
Results: Pulsatile retinal blood flow could be measured in all subjects. The mean and standard deviation of PI,RI, S/A ratio and D/A ratio were 1.30±0.16, 0.78±0.06, 1.65±0.08 and 0.35±0.08 respectively. The ICCs for the intra-observer repeatability and inter-observer reproducibility for pulsatile retinal blood flow parameters were greater than 0.926. The CORs were less than 10.97% for pulsatile retinal blood flow parameters except D/A ratio which was 20.51% for intra-observer repeatability and 18.15% for inter-observer reproducibility.
Conclusions: Doppler FD-OCT with phase-resolved algorithm is a rapid and reproducible method to measure pulsatile retinal blood flow. This method provides an alternative way to quantify retinal blood flow with Doppler-angle-independent flow indices that may provide insight on the retinal flow in many vascular related eye diseases.
Commercial Relationships: Meixiao Shen, None; **shenghai huang**, None; **Ce Shi**, None; **Fan Lu**, None
Support: the NationalMajorEquipmentProgramofChina(2012YQ12008004 to Lu), the National Nature Science Foundation of China (Grant No. 81170869 and 81570880 to Lu, Grant No. 81400441 to Shen)

Program Number: 462 **Poster Board Number:** A0099
Presentation Time: 1:30 PM–3:15 PM
Total Retinal Blood Flow Measurements with En Face Doppler Optical Coherence Tomography in Eyes with Central Retinal Vein Occlusion
Mark Lane[1, 2], ByungKun Lee[3], Nadia K. Waheed[2], Talisa E. de Carlo[2, 3], Mehreen Adhi[2], WooJhon Choi[3], Eric M. Moult[3], Jay S. Duker[2], James G. Fujimoto[3]. [1]Ophthalmology, Queen Elizabeth Hospital Birmingham, Birmingham, United Kingdom; [2]Tufts Medical Center, New England Eye Center, Boston, United Kingdom; [3]Electrical Engineering and Computer Science, Massachusetts Institute of Technology, Cambridge, MA.
Purpose: En face Doppler optical coherence tomography (OCT) enables fully automatic calculation of total retinal blood flow (TRBF) in the central retinal artery. The aim of this study was to validate this new technique in patients with central retinal vein occlusion (CRVO) and to investigate the role of TRBF in the pathophysiology of CRVO.
Methods: TRBF was measured in both eyes of six subjects (64.0±19.8yo, 5 females) that suffered from unilateral CRVO. TRBF was also measured in one randomly selected eye of nine age/sex matched normal control subjects (62.1±10.4yo, 7 females). TRBF was measured using a 1050-nm wavelength SS-OCT prototype operating at 400-kHz axial scan rate. Volumetric Doppler OCT image comprising 600×80 axial scans over a 1.5mm×2mm area at the optic disc was repeatedly acquired 24 times in 3.4 seconds of total scanning time. TRBF was calculated in each volume by automated analysis software and averaged over the cardiac cycle (Figure 1).
Results: Mean TRBF was 26.9±6.3μL/min in eyes with CRVO, 52.9± 18.3μL/min in the fellow eyes without vascular occlusion, and 43.5± 8.4μL/min in normal eyes. The TRBF was significantly lower in the eyes with CRVO compared to the normal fellow eye (P≤0.02, two-tailed Welch's t-test) and the age/sex matched control eyes (P≤0.001, two-tailed Welch's t-test). The mean TRBF was higher in the unaffected fellow eyes of the CRVO patients than in normal control eyes, however due to a large spread of TRBF in the fellow eyes, this was not statistically significant.
Conclusions: A statistically significant decrease in TRBF in eyes affected with CRVO was observed. Further work is required to ascertain if there is a significant increase in TRBF in the fellow eye of patients that suffer from CRVO compared to normal control subjects and to assess the use of this technology in screening patients that are at risk of CRVO, to allow early detection and targeted lifestyle modification.

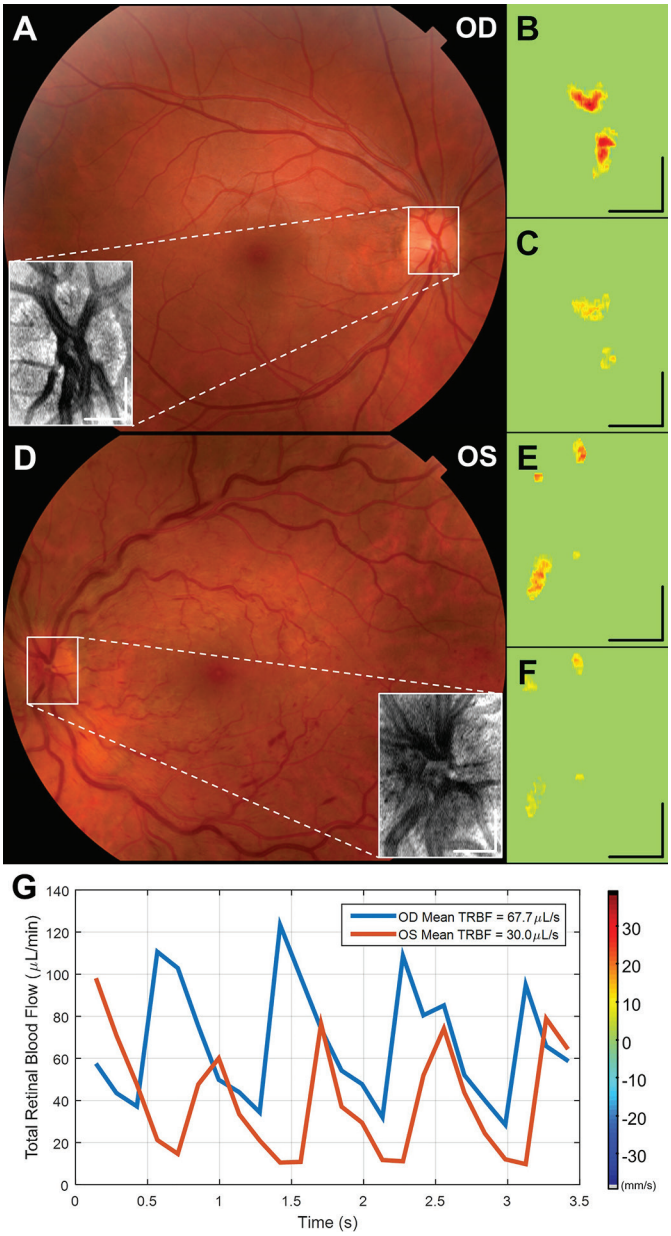

Fig. 1. TRBF measurement in a patient with unilateral CRVO. (A, D) *En face* Doppler OCT scan area marked on color fundus photographs. (B, C, E, F) Flow velocity *en face* profiles at systole and diastole. (G) Pulsatile TRBF in the two eyes. Scale bars 500μm.
Commercial Relationships: Mark Lane, None; **ByungKun Lee**, None; **Nadia K. Waheed**, OptoVue: Speaker (S), Thrombogenics: Speaker (S), Carl Zeiss Meditec: Research Support (F), Iconic therapeutics (C); **Talisa E. de Carlo**, None; **Mehreen Adhi**, None; **WooJhon Choi**, None; **Eric M. Moult**, None; **Jay S. Duker**, Topcon

Medical Systems Inc (C), Carl Zeiss Meditec Inc (C), Carl Zeiss Meditec Inc (F), Optovue (F), OptoVue (C); **James G. Fujimoto**, Optovue Inc. (I), Royalties from intellectual property owned by the Massachusetts Institute of Technology and licensed to Carl Zeiss Meditec Inc, Optovue (P)
Support: National Institutes of Health: R01-EY011289-29A, R44-EY022864, R01-CA075289-16. Air Force Office of Scientific Research: FA9550-15-1-0473, FA9550-12-1-0499

Program Number: 463 **Poster Board Number:** A0100
Presentation Time: 1:30 PM–3:15 PM
Quantitative Multifunctional OCT imaging of nonpathologic optic nerve head
Young-Joo Hong[1, 2], Aaron C. Chan[1, 2], Deepa Kasaragod[1, 2], Satoshi Sugiyama[1, 3], Shuichi Makita[1, 2], Yasushi Ikuno[4, 5], Masahiro Miura[6], Yoshiaki Yasuno[1, 2]. [1]Computational Optics Group, University of Tsukuba, Tsukuba, Japan; [2]Computational Optics and Ophthalmology Group, Tsukuba, Japan; [3]Tomey Corporation, Nagoya, Japan; [4]Ikuno Eye Center, Osaka, Japan; [5]Department of Ophthalmology, Osaka University, Suita, Japan; [6]Tokyo Medical University Ibaraki Medical Center, Ami, Japan.
Purpose: In order to investigate the tissue property of optic nerve head (ONH), quantitative optical coherence tomography (OCT) imaging was performed with 1-μm Jones-matrix multifunctional OCT (JM-OCT). This study aims at evaluating clinical utility of quantitative JM-OCT imaging, based on a descriptive normal ONH cases.
Methods: Five eyes of non-pathologic cases were imaged with quantitative JM-OCT. 3 mm × 3 mm areas around ONH were scanned with 512 × 1024 A-lines in 6.6 seconds. Intensity OCT, OCT signal attenuation coefficient (AC), complex correlation based OCT-angiography (OCA), local birefringence (LB) tomography, and degree-of-polarization-uniformity (DOPU) tomography were obtained from a volumetric scan. Each tomography represents the structure, combined coefficient of tissue scattering and absorption, vasculature, micro-structural property of tissue, and melanin, respectively. Contrast and properties of tissues in ONH are descriptively discussed.
Results: Fig. 1 shows an example of ONH with JM-OCT from high myopia. OCT projection (b) shows myopic conus. The conventional OCT intensity (a) shows moderate different intensity between prelamina (PL) and lamina cribrosa (LC) region. In contrast, the AC and LB images showed better discrimination of PL and LC. The log-scaled AC (d), LB (e), and correlation map (f) images shows high signal in LC relative to PL. The AC and LB images are less affected by upper tissue as shown in dashed loops region in (d,e). The DOPU (g) images show low value at the posterior of LC and peripapillary choroidal and scleral regions. Fig.1(h–m) show the *en face* slices of the AC (h, k), LB (i, l), and OCA (j, m) signals at the PL (h–j), and LC (k–m) regions. The difference between PL and LC is more clearly shown in the *en face* slice image as indicated with ellipses in (h–m). These observation was seen from all of five eyes.
The OCA projection (c) shows a portion of Zinn-Haller arterial circle (ZHAC, indicated with arrowhead) in the myopic conus. The ZHAC portion observed from two high myopic eyes (diopter: -8.50, -10.25).
Conclusions: The quantitative JM-OCT imaging gave clear discrimination of PL and LC with quantified values corresponding each tissue properties. The quantitative JM-OCT would enable quantitative assessment of in vivo ONH.

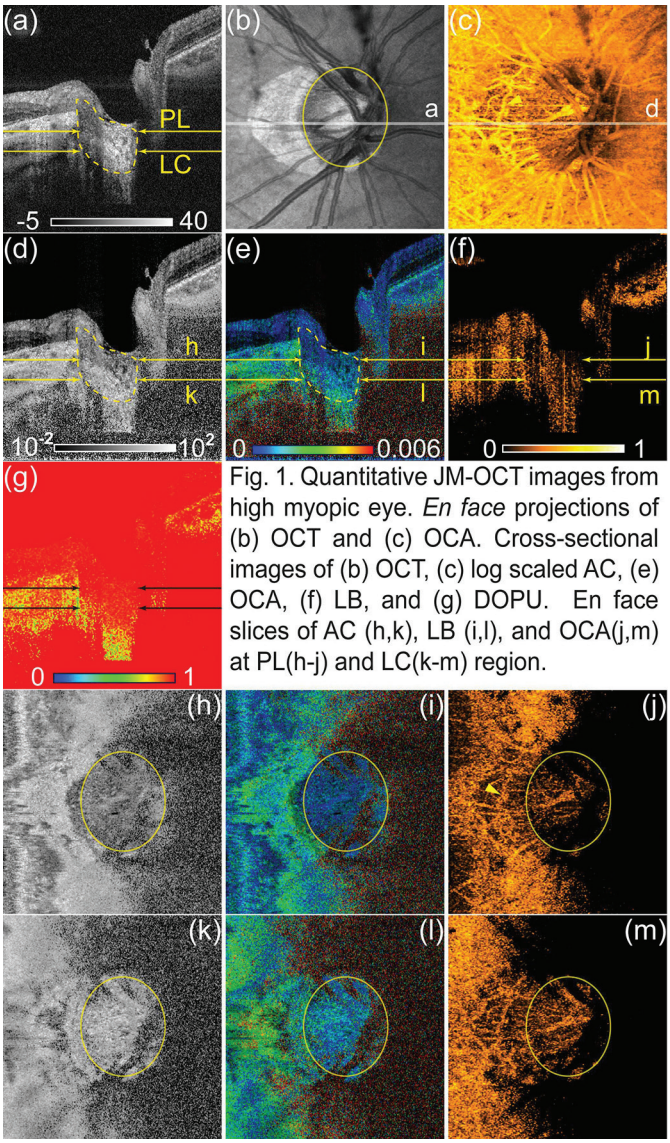

Fig. 1. Quantitative JM-OCT images from high myopic eye. *En face* projections of (b) OCT and (c) OCA. Cross-sectional images of (b) OCT, (c) log scaled AC, (e) OCA, (f) LB, and (g) DOPU. En face slices of AC (h,k), LB (i,l), and OCA(j,m) at PL(h-j) and LC(k-m) region.

Commercial Relationships: Young-Joo Hong, Nidek (F), Canon (F), Tomey Corp. (F), Topcon Corp. (F); **Aaron C. Chan**, Canon (F), Tomey Corp. (F), Topcon Corp. (F), Nidek (F); **Deepa Kasaragod**, Nidek (I), Topcon Corp. (F), Tomey Corp. (F), Canon (F); **Satoshi Sugiyama**, Tomey Corp.; **Shuichi Makita**, Nidek (F), Tomey Corp. (P), Topcon Corp. (F), Canon (F), Tomey Corp. (F); **Yasushi Ikuno**, Tomey Corp. (F); **Masahiro Miura**, NOVARTIS (F), BAYER (F), SANTEN (R), SANTEN (F), ALCON (F), NOVARTIS (R); **Yoshiaki Yasuno**, Tomey Corp. (P), Nidek (F), Topcon Corp. (F), Canon (F), Tomey Corp. (F)
Support: JSPS KAKENHI WAKATE B 15K20887

Program Number: 464 **Poster Board Number:** A0101
Presentation Time: 1:30 PM–3:15 PM
Sensitivity of Spectral Domain OCTA Imaging with Polarization and Beam defocus
Venu Manne, Patricia Sha, Jochen Straub, Mary K. Durbin. Carl Zeiss Meditec Inc., Dublin, CA.
Purpose: To demonstrate the effect of polarization and beam defocus/ocular diopter setting on image quality of Optical Coherence

Tomography Angiography(OCTA) scans acquired on CIRRUS HD-OCT Model 5000 (ZEISS Dublin, CA).
Methods: A commercial Cirrus HD-OCT Model 5000(ZEISS Dublin, CA) with software version 9.0 was used to acquire OCTA images on 5 eyes from healthy volunteers using OCTA 3x3 mm scan. For each eye the operator used the 'Autofocus ' and 'Optimize' features on the CIRRUS GUI to attempt to automatically find the optimal position to correct for refractive error and polarization, respectively. Using 'Autofocus ' and 'Optimize' features improves the scan image quality which is reflected in signal strength indicator for each scan. Signal strength ranges from 0 to 10, with 10 being maximum signal strength. From these optimal positions, the polarization paddle position was varied from 0 to 400 motor steps in steps of 50 and OCTA images were obtained at each step. Following that with optimal position for polarization, the ocular lens position was varied to correct for refractive error by +/-2.5 D in steps of 0.5 D, and OCT images were obtained at each step. FastTrack was used to maintain the scan position at the same location as the original optimized image.
Results: Based on data from 5 eyes, when varying the polarization position, the signal strength varied from as low as 4 to maximum of 10. When varying the beam diopter position, the signal strength varied little between 9 and 10. In Figure 1, the retinal vessels are more easily resolved and better defined with a scan of higher signal strength, see image (a) vs image (d) as pointed by red arrows. OCTA scans with signal strength of 8 or better showed highly detailed views of the retinal vasculature, even with 2.5D of defocus.
Conclusions: OCTA image quality is affected by polarization and beam defocus. The 'Autofocus ' and 'Enhance' features in CIRRUS(ZEISS Dublin, CA) serve to optimize signal strength and quality of OCTA scans.

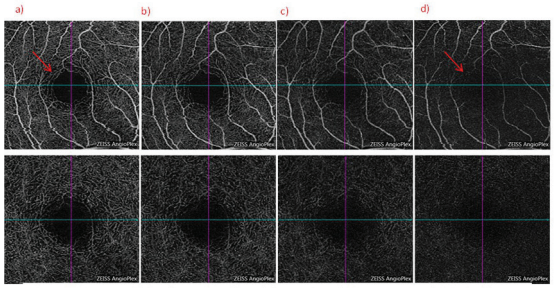

Figure 1. OCTA Retina Slab and Deep retina layer slab at varying polarization position a) 350, Signal Strength 10/10 b) 300 , Signal Strength 9/10 c) 150, Signal Strength 7/10 d) 250, Signal Strength 5/10

Commercial Relationships: Venu Manne, Carl Zeiss Meditec; **Patricia Sha**, Carl Zeiss Meditec; **Jochen Straub**, Carl Zeiss Meditec; **Mary K. Durbin**, Carl Zeiss Meditec

Program Number: 465 **Poster Board Number:** A0102
Presentation Time: 1:30 PM–3:15 PM
Ellipsoid Zone Thickness Measured by Ultrahigh Resolution Spectral-Domain Optical Coherence Tomography
Yoshitsugu Matsui[1], Masaharu Mizuochi[2], Eriko Uchiyama[3], Mineo Kondo[3]. [1]Ophthalmology, Okanami general hospital, Iga, Japan; [2]Kowa company, Ltd, Chuo-ku, Japan; [3]Mie university graduated school of medicine, Tsu, Japan.
Purpose: Spaide made scale drawings of the outer retina based on histological findings. It is possible to compare the drawings with OCT images using a longitudinal reflectivity profile (LRP) analysis. In the comparison, band 2 was aligned with the ellipsoid of the model. In contrast, the LRP of the IS/OS boundary reached a trough. But the comparison was made by using standard resolution SD-OCT. An ultrahigh resolution (UHR) SD-OCT can provide additional information to that provided by standard-resolution SD-OCT. We compared the thickness of the ellipsoid zone (EZ) obtained by a prototype UHR-SD-OCT with that obtained by a standard-resolution SD-OCT.
Methods: Twenty-six eyes of 26 healthy volunteers were studied. B-scan images through the fovea were obtained by the two different OCT machines. We created LRP from the B-scan images. We majored the width of EZ at the 75% of the maximum reflectiveness at five points; a position of central fovea, a 0.5mm and 1.0mm temporal position from central fovea, a 0.5mm and 1.0mm nasal position from central fovea. And we compared the outer retina drawings with the UHR-SD-OCT images using the LRP analysis.
Results: In the standard resolution SD-OCT, the full width at 75% of the maximum reflectiveness of EZ was 16.50±0.53 μm at the fovea, 16.65±0.45 μm at 0.5 mm temporal to the fovea, 15.90±0.47 μm at 0.5 mm nasal to the fovea, 16.80±0.35 μm at 1.0 mm temporal to the fovea, and 16.65±0.54 μm at 1.0 mm nasal to the fovea. In the UHR-SD-OCT, the full width at 75% of the maximum reflectiveness of the EZ was 7.30±0.60 μm at the fovea, 6.75±0.23 μm at 0.5 mm temporal to the fovea, 7.15±0.33 μm at 0.5 mm nasal to the fovea, 7.15±0.30 μm at 1.0 mm temporal to the fovea, and 6.40±0.37 μm at 1.0 mm nasal to the fovea. The full width at 75% of the maximum reflectiveness in the UHR-SD-OCT image was significantly thinner than that of the SD-OCT image at each of the five regions. In our comparisons, Band 2 was aligned with the distal ends of the ellipsoid section and/or the IS/OS boundary of the scale model.
Conclusions: The macular EZ thickness in UHR-SD-OCT images was <45% of that in SD-OCT images. The band2 was aligned with the distal ends of the ellipsoid section and/or the IS/OS boundary of the scale model. While a drawing is not likely to be the final arbiter of band assignments, further studies are needs to determine the origin of band 2.

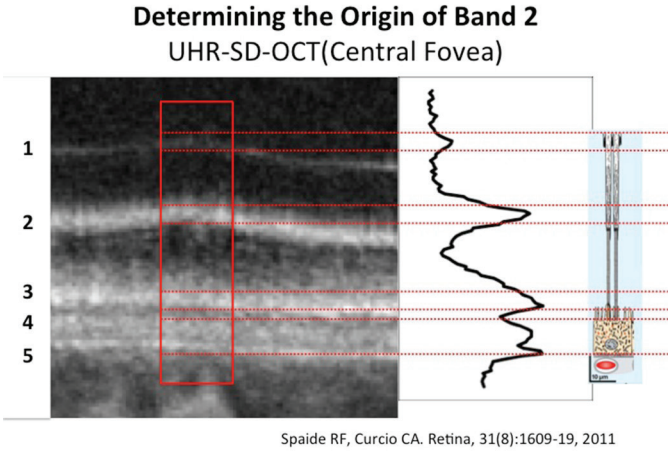

Spaide RF, Curcio CA. Retina, 31(8):1609-19, 2011

Commercial Relationships: Yoshitsugu Matsui; **Masaharu Mizuochi**, Kowa company, Ltd; **Eriko Uchiyama**, Kowa company, Ltd (F); **Mineo Kondo**, Kowa company, Ltd (F)

Program Number: 466 **Poster Board Number:** A0103
Presentation Time: 1:30 PM–3:15 PM

Ultrahigh Speed Ophthalmic Surgical OCT for Intraoperative OCT Angiography and Widefield Imaging

Chen D. Lu[1], Andre J. Witkin[2], Nadia K. Waheed[2], Benjamin Potsaid[1, 3], Jonathan J. Liu[4], Eric M. Moult[1], Vijaysekhar Jayaraman[5], Kinpui Chan[4], Jay S. Duker[2], James G. Fujimoto[1]. [1]Research Laboratory of Electronics and Department of Electrical Engineering and Computer Science, Massachusetts Institute of Technology, Cambridge, MA; [2]New England Eye Center and Tufts Medical Center, Tufts University, Boston, MA; [3]Thorlabs, Inc., Newton, NJ; [4]Topcon Medical Systems, Inc., Oakland, NJ; [5]Praevium Research, Inc., Santa Barbara, CA.

Purpose: Ultrahigh speed optical coherence tomography (OCT) enables functional imaging such as OCT angiography (OCTA) that require repeated scanning and widefield imaging with densely sampled data sets. We have developed an ultrahigh speed OCT system with a scanner attachment that shares the optical path of a surgical microscope, enabling compatibility among varying microscope models.

Methods: The galvanometer-based OCT module was attached to the Topcon OMS-800 microscope below the objective lens (Fig. 1A). The OCT system uses a 400 kHz, 1050 nm wavelength vertical cavity surface emitting laser (VCSEL) swept source with 80 nm sweep length and ~8 µm axial resolution in tissue. The measured optical power was within the 1.9 mW safety limit. OCTA was performed with 500x500 A-scan, 5 repeated B-scan volumes acquired in 3.6 s. Widefield 1000x1000 A-scan volumes were acquired in 2.9 s. The OCT data was acquired during surgery and reviewed postoperatively.

Results: Fig. 1B-F shows 6x6 mm^2 OCTA and structural OCT data from an 82-year-old patient during epiretinal membrane surgery. Imaging was performed with an 80D Topcon OFFISS non-contact lens. OCTA was also performed using a GRIESHABER DSP contact lens (Fig. 2A-E). By increasing the scan range, the 80D lens allowed for a 12x12 mm^2 widefield OCT volume (Fig. 2F-H) of the same patient. The OCT system is capable of assessing anterior ocular structures during cataract surgery of a 72-year-old patient (Fig. 2I-K).

Conclusions: Ultrahigh speed will improve the OCT data quality and bring functional and widefield imaging to the surgical suite. For future work, we will utilize GPU processing for real-time OCT feedback.

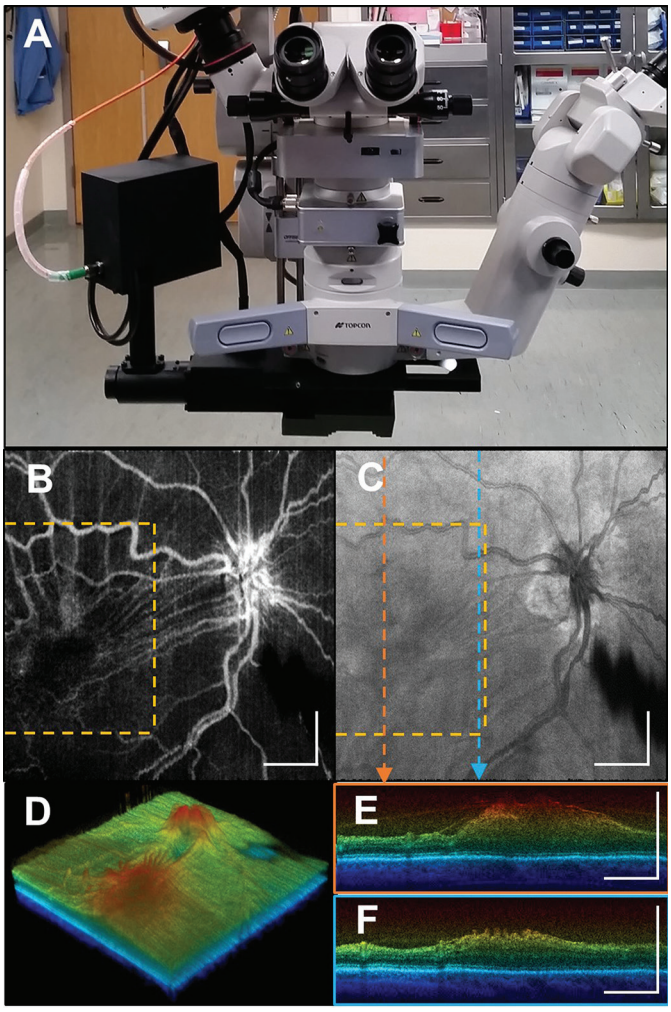

Fig. 1 (A) The OCT scanner attachment to the Topcon OMS-800 surgical scope. (B) 6x6 mm^2 OCTA and (C) structural en-face projections, (D) depth color-encoded flattened 3D rendering, and (E-F) 5 averaged cross sections acquired through an 80D OFFISS lens during epiretinal membrane surgery. Scale bars: 1 mm.

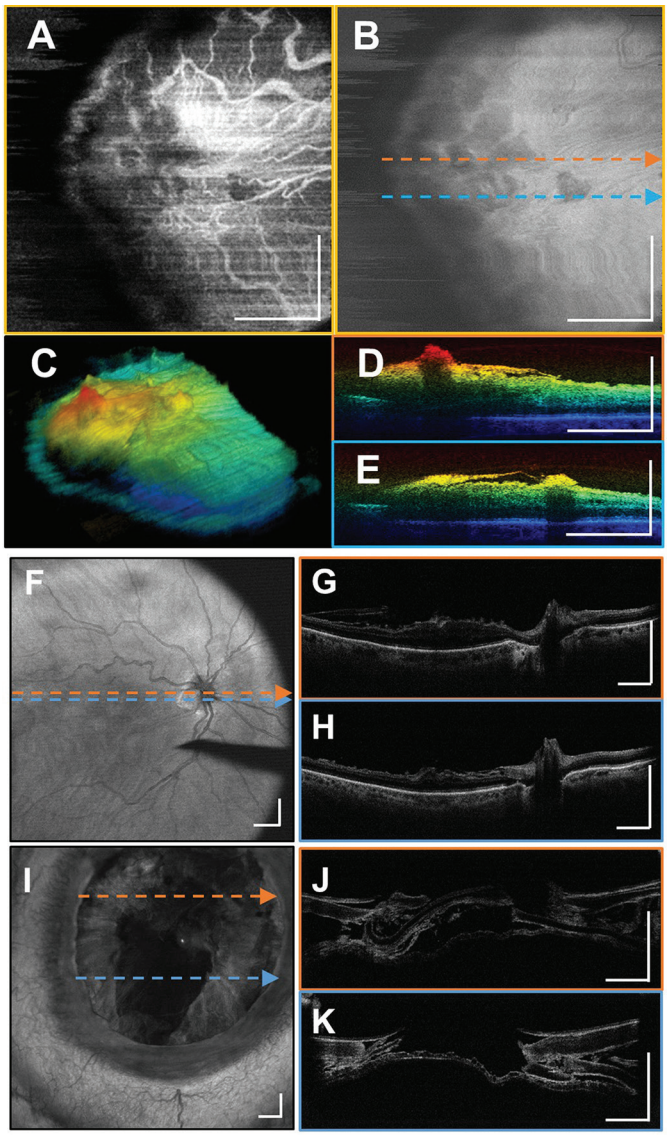

Fig. 2 (A) 3.8x3.8 mm^2 OCTA and (B) structural enface projections, (C) depth color-encoded flattened 3D rendering, and (D-E) cross-sections acquired with a contact lens. (F) Widefield 12x12 mm^2 structural enface projection and (G-H) cross-sections through an 80D OFFISS lens. (I) Structural enface of the anterior eye with (J-K) cross-sections of the lens capsule. All cross-sections were averaged 5 times. Scale bars: 1 mm.

Commercial Relationships: **Chen D. Lu**, None; **Andre J. Witkin**, None; **Nadia K. Waheed**, Iconic Therapeutics (C), ThromboGenics (C), Carl Zeiss Meditech, Inc. (F); **Benjamin Potsaid**, Thorlabs, Inc. (P), Thorlabs, Inc.; **Jonathan J. Liu**; **Eric M. Moult**, None; **Vijaysekhar Jayaraman**, Praevium Research, Inc., Thorlabs, Inc. (P), Thorlabs, Inc. (F); **Kinpui Chan**, Topcon Medical Systems, Inc.; **Jay S. Duker**, Optovue, Inc. (C), Carl Zeiss Meditech, Inc. (F), Carl Zeiss Meditech, Inc. (C), Optovue, Inc. (F); **James G. Fujimoto**, Optovue, Inc. (P), Optovue, Inc. (I), Carl Zeiss Meditech, Inc. (P)
Support: NIH 5-R01-EY011289-29A, R44-EY022864-02; AFOSR FA9550-12-1-0499, FA9550-15-1-0473

Program Number: 467 **Poster Board Number:** A0104
Presentation Time: 1:30 PM–3:15 PM

4D Microscope-Integrated OCT to Visualize Depth-Related Steps During Anterior Segment and External Eye Procedures

Paramjit K. Bhullar[1], Neel D. Pasricha[1], Oscar M. Zevallos-Carrasco[2], Christian Viehland[2], Brenton Keller[2], Melissa B. Daluvoy[1], Pratap Challa[1], Sharon F. Freedman[1], Joseph A. Izatt[2, 1], Cynthia A. Toth[1, 2], Anthony N. Kuo[1].
[1]Ophthalmology, Duke University School of Medicine, Durham, NC; [2]Biomedical Engineering, Duke University, Durham, NC.

Purpose: Several ophthalmic surgical procedures require accurate assessment of instrument depth, which can be challenging from a standard top-down view of the surgical field. Using live intraoperative 4D (3D across time) swept-source microscope-integrated optical coherence tomography (SS-MIOCT), we demonstrate direct visualization of depth-related steps in glaucoma, strabismus, and corneal surgeries.
Methods: Six subjects undergoing tube shunt placement, trabeculectomy, iStent placement, lateral rectus resection, Descemet's stripping automated endothelial keratoplasty (DSAEK), and deep anterior lamellar keratoplasty (DALK) were consented under a Duke IRB approved protocol. A 100kHz SS-MIOCT system with a volume rate of 2Hz was used to visualize key depth related steps intraoperatively, in real-time.
Results: SS-MIOCT provided surgeons with live guidance and visualized scleral tunneling, tube shunt positioning in the anterior chamber (AC), and suturing during tube shunt placement; scleral flap creation, sclerotomy, and iridectomy during trabeculectomy; positioning of stent in area of Schlemm's canal during iStent placement; needle depth during muscle and scleral passes during strabismus surgery; fluid between graft and native cornea during DSAEK; and needle depth in cornea prior to air injection during DALK. Select images are shown in Fig. 1.
Conclusions: Assessment of instrument depth in the AC, sclera, muscle, and cornea can be challenging during ophthalmic procedures, but is important in avoiding complications such as inadequate reductions in intraocular pressure due to suboptimal positioning of drainage devices, muscle slipping and scleral perforation during strabismus surgery, non-adherence of the donor and native corneas during DSAEK, and unsuccessful big-bubble formation during DALK. SS-MIOCT allows for visual guidance of depth-based steps in real-time, making it a valuable tool for ophthalmic surgeons.

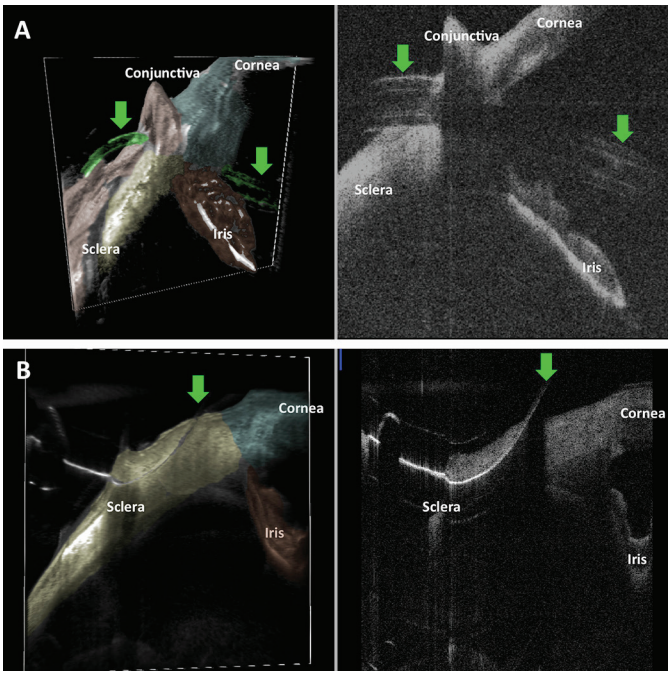

SS-MIOCT volumetric (left, with manual false coloring) and B-scan (right) pairs showing (A) tube (green arrows) during tube shunt placement and (B) needle (green arrow) depth in sclera during strabismus surgery.

Commercial Relationships: Paramjit K. Bhullar; **Neel D. Pasricha**, None; **Oscar M. Zevallos-Carrasco**, None; **Christian Viehland**, None; **Brenton Keller**, None; **Melissa B. Daluvoy**, None; **Pratap Challa**, None; **Sharon F. Freedman**, None; **Joseph A. Izatt**, Bioptigen (S), Bioptigen (P), Bioptigen (I); **Cynthia A. Toth**, Bioptigen (F), Duke University (P), Alcon (F), ThromboGenics (C), Genentech (F); **Anthony N. Kuo**, Bioptigen (P)

Support: National Institutes of Health Bioengineering Research Partnership Grant R01-EY023039, National Institutes of Health R01-EY024312, and unrestricted grant from Research to Prevent Blindness to the Department of Ophthalmology at Duke University School of Medicine

Clinical Trial: NCT01588041

Program Number: 468 **Poster Board Number:** A0105
Presentation Time: 1:30 PM–3:15 PM

Multimodal imaging including intraoperative optical coherence tomography (OCT) and en face OCT to visualize immediate effect and extent of internal limiting membrane (ILM) peeling in macular hole surgery

Steven J. Ryder, Justin Townsend. Ophthalmology, Bascom Palmer Eye Institute, Miami, FL.

Purpose: Internal limiting membrane (ILM) peeling has been shown to improve the anatomical and visual outcomes in macular hole repair. The purpose of this report is to illustrate the benefit of intraoperative OCT and en face OCT an eye undergoing pars plana vitrectomy with ILM peeling. Intraoperative OCT can demonstrate immediate improvement in foveal contour while en face OCT is a novel modality to assess extent of ILM peeling following macular hole surgery.

Methods: A fifty-four year old Caucasian female with a full-thickness macular hole in her right eye underwent pars plana vitrectomy, ILM peeling, fluid-air exchange and 25% SF6 gas injection in her right eye. Intraoperative OCT images were recorded with the ZEISS OPMI LUMERA 700 and RESCAN 700. Postoperative en face OCT images were recorded with the Cirrus HD-OCT 5000.

Results: Preoperative visual acuity was 20/200 in the right eye with a full-thickness macular hole. Following complete vitrectomy and staining of the ILM with indocyanine green, the ILM was peeled to a radius of at least two disc diameters and out to the vascular arcades. Intraoperative OCT immediately following ILM peel demonstrates marked improvement in the macular hole contour due to release of tractional forces. With the hole completely closed at postoperative day eight, the area of peeled ILM is highligted well by en face OCT. The hole closed entired Visual acuity improved to 20/50 at one month following surgery.

Conclusions: Intraoperative OCT and postoperative en face OCT are uniquely equipped to visualize the immediate effect of ILM peeling and confirm adequate removal, respectively.

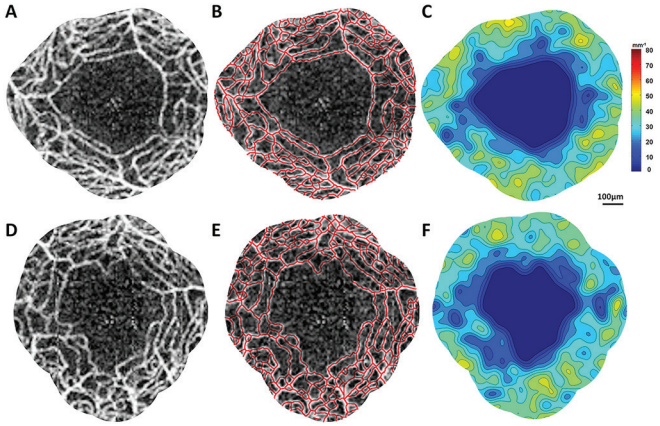

Image 1. Intraoperative OCT before and immediately following ILM peeling. There is marked improvement in foveal contour and scattered small superficial flame hemorrhages above the retinal nerve fiber layer (orange arrows).

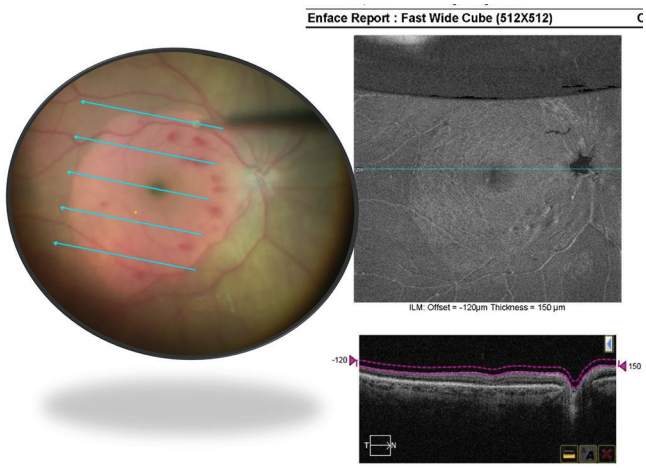

Image 2. A distinctly different shade of gray highlights the extent of the ILM peeling in this postoperative day 8 en face OCT (right) and correlates well with an intraoperative photograph immediately following peel (left).

Commercial Relationships: Steven J. Ryder, None; **Justin Townsend**, None

Program Number: 469 **Poster Board Number:** A0106
Presentation Time: 1:30 PM–3:15 PM
Imaging of Pediatric Retinal Pathology with Long Working Distance Swept Source Optical Coherence Tomography
Ruobing Qian[1], Oscar Carrasco-Zevallos[1], Shwetha Mangalesh[2], Neeru Sarin[2], Lejla Vajzovic[2], Cynthia A. Toth[2, 1], Joseph A. Izatt[1, 2].
[1]Biomedical Engineering, Duke University, Durham, NC; [2]Ophthalmology, Duke University Medical Center, Durham, NC.
Purpose: Conventional optical coherence tomography (OCT) systems have working distances of about 25 mm, and require a chin rest to immobilize the patients. However, imaging young children is challenging due to their lack of attention and inherent fear of large objects close to their face. In this work, we describe a novel 2f OCT system with a long working distance (from the last optical element to the subject's eye) of 348mm, and demonstrate its utility for adult and pediatric subjects with retinal pathology.
Methods: An optical schematic of the novel 2f scanning configuration of the OCT sample arm is shown in Fig.1 (a). The optical design and performance of the system was detailed previously (*Invest. Ophthalmol. Vis. Sci.* 2015; 56(7):4094). The objective lens L_2 with f=250mm, results in a working distance of 348mm. An iris camera was used to facilitate subject alignment by placement of the subject's iris centered on a dot on the camera images. Images were captured either with (mounted on a slit lamp base, to align with the system) or without a chin rest (gently holding the subject's head) supporting the subject [Fig 1 (b)]. B-scans, volumetric images of the fovea and optic nerve were obtained.
Results: 26 adult subjects (10 with and 16 without retinal disease) and 4 children aged 13-17 (2 with and 2 without retinal disease) were imaged under a Duke Medical Center IRB protocol. Representative images from both adults and children are shown in Fig.2.
Conclusions: We have demonstrated for the first time the use of a novel 2f OCT system with a long working distance of 348mm for imaging adults and children with and without retinal pathology and with and without pupil dilation. This optical design may have significant advantages for imaging patients who are unable to cooperate with a system near their face.

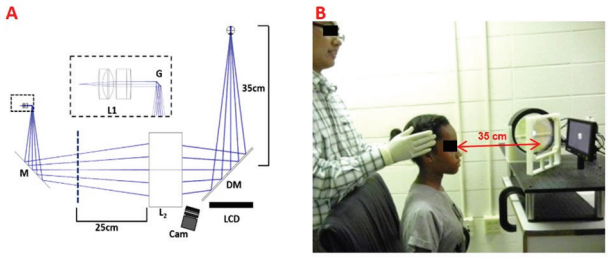

Fig.1 A: Schematic of the OCT sample arm and subject alignment system. L1, L2: custom lenses; DM: dichroic mirror; G: galvanometer mirror pair; M: first surface mirror; LCD: LCD fixation target monitor; Cam: iris camera; B: 13 year old girl being aligned without a chin rest to the OCT system

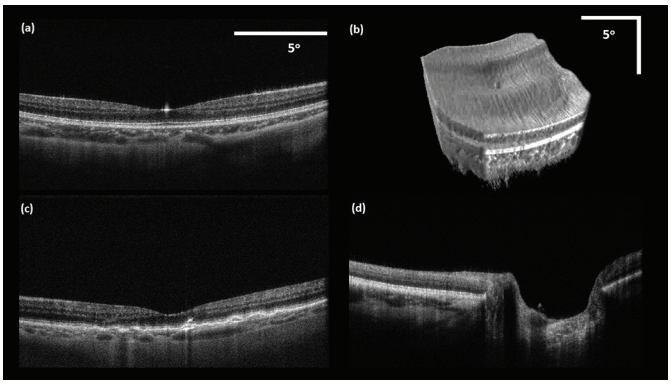

Fig.2 (a) B-scan from an undilated 14 year old child, and (b) corresponding volumetric foveal scan. (c) B-scan from a 79 year old dilated adult subject with RPE elevation. (d) B-scan from a dialated 16 year old child with juvenile idiopathic arthritis and bilateral optic nerve cupping. All B-scans 10x averaged.
Commercial Relationships: Ruobing Qian; **Oscar Carrasco-Zevallos**, None; **Shwetha Mangalesh**, None; **Neeru Sarin**, None; **Lejla Vajzovic**, None; **Cynthia A. Toth**, Thrombogenics (C), Alcon (P), Genetech (F), Bioptigen (F); **Joseph A. Izatt**, None
Support: The Hartwell Foundation
Clinical Trial: NCT02582164

Program Number: 470 **Poster Board Number:** A0107
Presentation Time: 1:30 PM–3:15 PM
Retinal imaging with full-field optical coherence microscopy
Kate Grieve[1, 2], Vincent Borderie[1, 2], Michel Paques[1, 2]. [1]Institut de la Vision, Paris, France; [2]Quinze Vingts Ophthalmology Hospital, Paris, France.
Purpose: To interpret full-field optical coherence microscopy (FFOCM) images of ex vivo retina.
Methods: Images of flatmounted retinas of human, primate, pig, sheep, rat, mouse and zebrafish were acquired using FFOCM. For identification of ganglion cells, samples immunolabelled against Tuj1 and Brn3a were analyzed by combining FFOCM, fluorescence confocal microscopy (FCM) and fluorescence-FFOCM. To investigate post-mortem tissue changes, time series were acquired on primate retina over 48 hours and on fresh versus fixed tissue.
Results: With FFOCM, cell types and features such as nerve fiber bundles and RGC somas were resolved without use of contrast agents at 1µm xyz resolution. RGC somas in large mammals appeared bright with dark contours, while in rodents RGC somas appeared dark with bright contours. RGC axon to soma junctions could be traced in the 3D image stacks. Time series revealed undulation of retinal tissue samples over 48 hours, though no degradation of individual cells was detected, while paraformaldehyde fixation caused increased scattering and shrinkage.
Conclusions: FFOCM reveals micrometric morphological detail in the retina without the use of contrast agents. We observed interspecies differences in optical properties of RGC somas. Fixation significantly alters retinal transparency hence reducing the visibility of microscopic features.

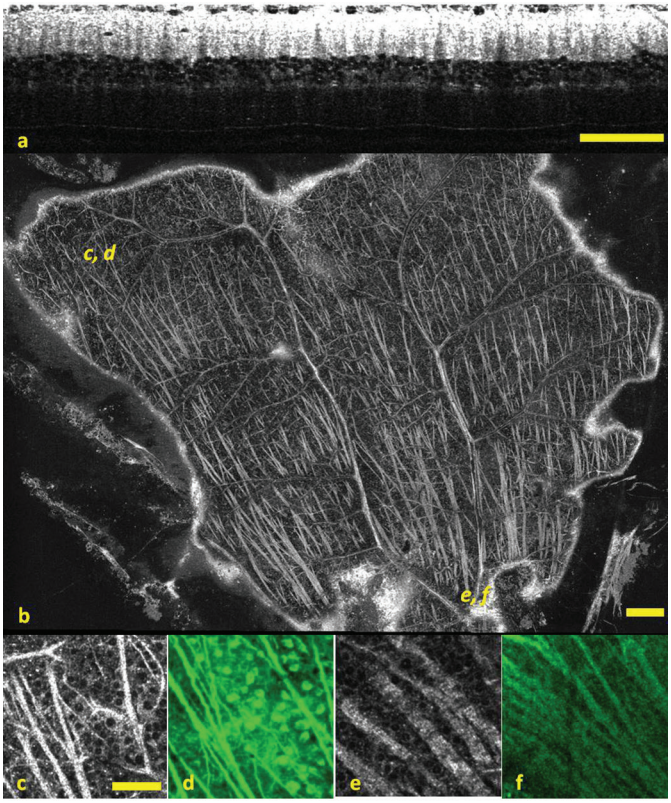

Rat retina in FFOCM and FCM. *a* cross-section; *b* wide field mosaic of flat-mounted section of rat retina with optic nerve located at the bottom of the image and the periphery at the top, with letters indicating locations of zoomed zones *c-f*; *c* zoom on peripheral zone with FFOCM and *d* similar zone in FCM with Tuj1 staining reveal axons and cells; *e* zoom on zone close to optic nerve with FFOCM and *f* with FCM with Tuj1 staining reveal axon bundles. In FFOCM, axons are bright and cells are dark centered, bright contoured. Scale bar *a* 100µm; *b* 200µm, *c-f* 50µm.

Commercial Relationships: Kate Grieve, None; **Vincent Borderie**; **Michel Paques**, None

Support: European Research Council SYNERGY Grant scheme (HELMHOLTZ, ERC Grant Agreement # 610110) and Agence Nationale de Recherche (ANR), under a PRTS (Projet de Recherche Translationelle en Santé) grant (ANR-13-PRTS-0009)

Program Number: 471 **Poster Board Number:** A0108
Presentation Time: 1:30 PM–3:15 PM

Dual-band optical coherence tomography using a single supercontinuum laser source

Siyu Chen[1], Xiao Shu[1], Ji Yi[1, 2], Amani A. Fawzi[3], Hao F. Zhang[1, 3].
[1]Biomedical Engineering, Northwestern University, Evanston, IL; [2]Department of Medicine, Boston University, Boston, MA; [3]Department of Ophthalmology, Northwestern University, Chicago, IL.

Purpose: Though blood oxygen saturation (sO_2) is a vital physiological indicator, OCT using near infrared (NIR) may not measure it accurately. Visible (Vis-) OCT can address the problem. However, concerns over its imaging capability still remains. We seek to answer this question by construction a dual-band OCT system, comparing them side-by-side.

Methods: A supercontinuum laser served as light source. We separated and delivered visible and NIR light to two interferometers. We employed free-space configuration for the visible interferometer. The NIR-OCT used the traditional fiber-based design. The two beams were recombined before entering the scanning mechanism, so the images were co-registered.

We imaged mouse retina *in vivo*. In addition to structure images, we generated OCT angiography using complex de-correlation. Dual-ring scanning allowed us to measure retinal blood flow. Finally, we used spectral fitting to extract (sO_2) from major retina vessels.

Results: Our Vis- and NIR-OCT subsystems achieved depth resolution of 1.8 and 4.4 µm, respectively. Both structural images showed similar features. They also rendered the same retinal vascular network topography. We overlaid OCT angiography with structural B-scans and confirmed their physiological distribution. Besides similarities, the higher resolution of vis-OCT emphasized the fibrous features in the neural fiber layer. It also offered better separation between retinal layers.

Blood flow measurements showed comparable results among two subsystems. The total flow rate was 2.71±0.27 and 2.53±0.27 µL/min for arteries and veins in Vis-OCT, respectively. NIR-OCT gave us 2.76±0.17 and 2.52±0.17 µL/min, respectively. No statistical difference was found between the values, further confirming our measurements.

We successfully extracted sO_2 from vis-OCT. The averaged arterial and venous sO_2 was 98±3% and = 85±3%, respectively. However, we failed to extract sO_2 from NIR-OCT using the same method. The relative weak absorption and strong scattering did not provide enough contrast to differentiate the two hemoglobin states.

Conclusions: We demonstrated a vis-/NIR dual-band OCT system capable of simultaneous imaging. The two systems have comparable performance in structural imaging, angiography and blood flow measurements. However, vis-OCT has higher resolution and further enables sO_2 extraction.

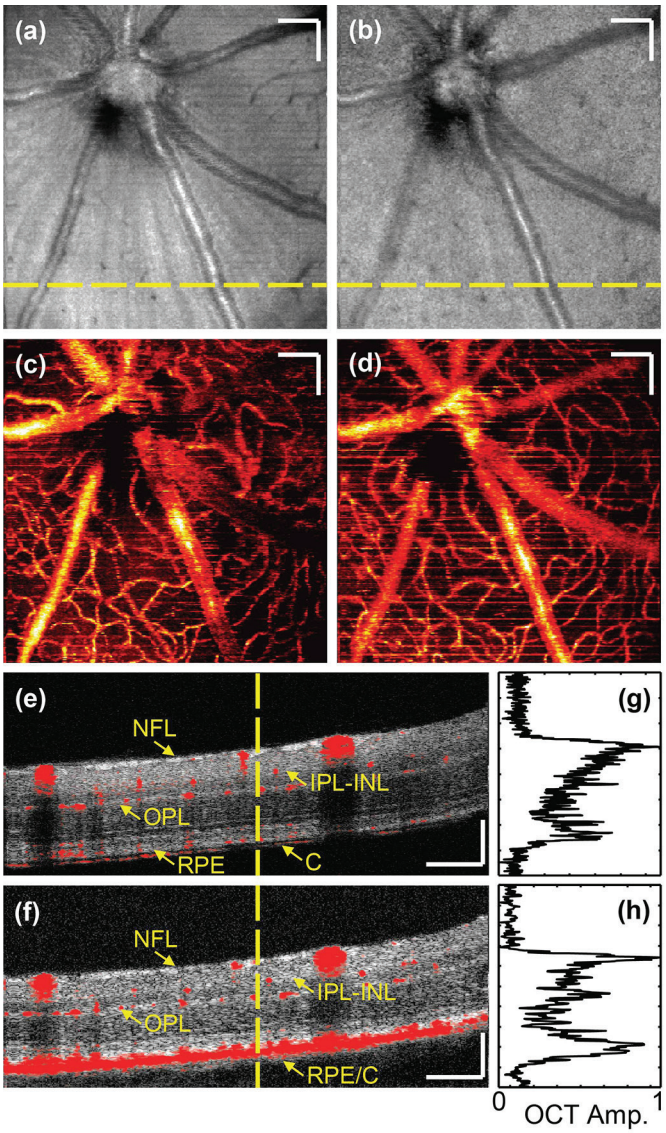

C: Choroid; IPL-INL: inner plexiform and inner nuclear layer; NFL: neural fiber layer; OPL: outer plexiform layer; RPE: retinal pigment epithelium. Scale: 100 µm.

Comparison of Vis- and NIR-OCT. (a, c, e, g) Vis-OCT images. (b, d, f, h) NIR-OCT images.

Commercial Relationships: Siyu Chen, None; **Xiao Shu**; **Ji Yi**, None; **Amani A. Fawzi**, None; **Hao F. Zhang**, None
Support: NIH Grants 1R01EY019951, 1R24EY022883, and 1DP3DK108248, NSF Grant CBET-1055379.

Program Number: 472 **Poster Board Number:** A0109
Presentation Time: 1:30 PM–3:15 PM

Localized absorption measurements for possible oxygen saturation using visible-light spectroscopic optical coherence tomography

Ranjan Rajendram[1, 4], Felix Fleischhauer[2, 3], Sophie Caujolle[2, 3], Michael Maria[2, 3], Thomas Feuchter[3], Lasse Leick[3], Adrian Podoleanu[2]. [1]Retina Research, UCL Institute of Ophthalmology, London, United Kingdom; [2]Applied Optics Group, University of Kent, Canterbury, United Kingdom; [3]NKT Photonics, Birkeroed, Denmark; [4]Moorfields Eye Hospital, London, United Kingdom.

Purpose: Spectroscopic optical coherence tomography (SOCT) combines imaging of optical coherence tomography (OCT) with localized absorption, which is used as functional information. By covering the spectral range from 490 to 730 nm a powerful tool to measure localized (de-)oxygenated hemoglobin for oxygen saturation estimation is being developed. This can be used in applications, such as retinal venous and arteriolar occlusions, diabetic retinopathy, glaucoma or assessment of central venous and arteriolar oxygen saturation.

Methods: Using a spectrometer based OCT, one has direct access to wavelength information. The measured spectrum is divided in 8 spectral windows, covering unique parts of the spectrum, and the OCT data are processed on each window separately and a cross link between spectral and structural information is obtained. Measurements are done with a 1:1, 1:2, 1:3, 1:10 and 1:100 concentration of Rhodamine B to ethanol, filled in a 50 µm cuvette and its attenuation is measured and compared to literature. Front and back surface of the cuvette are used and their amplitude compared. The attenuation for each window is calculated and used to estimate the absorption of the spectral windows. The OCT signal is attenuated by scattering, absorption and signal decay over imaging depth (roll-off). Rhodamine B is chosen because of its similar absorption peak, around 542 nm, as hemoglobin.

Results: The measurements show that SOCT can be used to reconstruct the absorption maximum of Rhodamine B, but the accuracy degrades with fading concentration (see Fig. 1 and 2). The 1:100 concentration shows false results, which means that we have overcome the sensitivity of our set-up.

Conclusions: We can show that using SOCT can be used to find the absorption maximum of Rhodamine B and the signal degrades with thinner solutions.

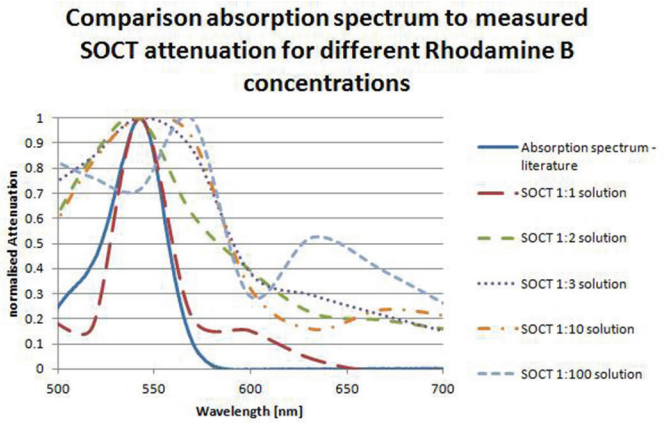

Comparison of Rhodamine B absorption spectrum to SOCT measured attenuation using different concentrations. The measurements show that SOCT can be used to reconstruct the absorption maximum of Rhodamine B, but the accuracy degrades with fading concentration. Due to smaller attenuation at 542 nm the peak width appear broader.

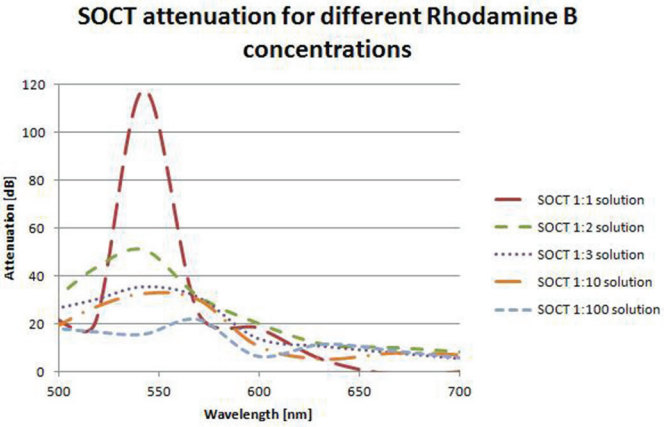

Measured attenuation with SOCT for different solutions. A high Rhodamine B concentration results in a higher attenuation in the OCT signal around 542 nm. Attenuation in OCT signal is caused by roll-off, scattering and absorption.

Commercial Relationships: Ranjan Rajendram, None; **Felix Fleischhauer**, NKT Photonics; **Sophie Caujolle**, NKT Photonics; **Michael Maria**, NKT Photonics; **Thomas Feuchter**, NKT Photonics; **Lasse Leick**, NKT Photonics; **Adrian Podoleanu**

Program Number: 473 **Poster Board Number:** A0110
Presentation Time: 1:30 PM–3:15 PM
Spectralis SD-OCT fovea to disc alignment technology versus anatomic positioning system in healthy population

Lorena Solé González[1], Rodrigo Abreu-González[1], Marta Alonso Plasencia[1], Pedro Abreu-González[1], Jose Augusto Abreu Reyes[2]. [1]University Hospital of La Candelaria, Santa Cruz de Tenerife, Spain; [2]University Hospital of Canarias, La Laguna, Spain.

Purpose: The aim of the present study is to evaluate differences between Spectralis SD-OCT fovea to disc alignment technology (FoDi) versus anatomic positioning system (APS) in healthy population. The Spectralis SD-OCT FoDi system, using TruTrack™ technology, automatically tracks and aligns 12° circle scans with a center manually positioned on confocal laser image of the optic nerve head. APS aligns scans automatically in relation to the patient's individual Fovea-to-Bruch's Membrane Opening centers axis. Both improve reproducibility eliminating rotational artifacts during scanning

Methods: Prospective observational study in 37 eyes of 20 healthy subjects without ocular disease. Each participant underwent a comprehensive ophthalmologic examination. Spherical equivalent inclusion criteria were between -5.0 D and +5.0 dioptres. Measurements of the peripapilar RNFL thickness were obtained, in one session, without pupil dilatation. The same experienced operator carried out all exams, and adjusted the automatic detection of Bruch's membrane opening. All images with artifacts and errors on RNFL segmentation were excluded from the analysis.

Results: RNFL average thickness measurements were 102.86±7.57 microns (FoDI) and 104.91±8.34 microns (APS) showing statistical significance (p=.039). Only superior temporal and inferior nasal RNFL diagram sectors showed no statistical significance (p>.05). Ocular torsion did not differ between both examinations (p=.886). Diameter discrepancies were very small, the mean diameter for the fixed 12° circles was 3.55 ± 0.12 mm, and the mean degree for the fixed 3.5 mm circles was 11.87±0.41°. The agreement among RNFL measurements obtained by the different protocols of the same instrument was investigated using regression analysis, Bland-Altman plots and a paired T-test.

Conclusions: Our results indicate that Spectralis SD-OCT RNFL thickness measurements using FoDi and APS showed different values, so they are not interchangeable. Whereas the definitions of the diameters are different in both protocols, the position of the circles and their sizes are very similar and the underlying biological structure usually did not change abruptly. The major reason for changes in the measurements between these circles are vessels near section borders, which changes the section from one to the other circle or differences in the segmentation lines.

Commercial Relationships: Lorena Solé González, None; **Rodrigo Abreu-González**; **Marta Alonso Plasencia**, None; **Pedro Abreu-González**, None; **Jose Augusto Abreu Reyes**, None

Program Number: 474 **Poster Board Number:** A0111
Presentation Time: 1:30 PM–3:15 PM
12% fat milk as OCT contrast agent for ex vivo imaging

Christian van Oterendorp[1], Viktoria Mans[1], Charlotte Fischer[1], Mohammed Khattab[1], Thomas Wecker[2]. [1]Dpt. of Ophthalmology, University of Goettingen, Göttingen, Germany; [2]Eye Center, University of Freiburg, Freiburg, Germany.

Purpose: Contrast agents applicable for optical coherence tomography (OCT) imaging are rare. Among them, gold nanorods are best characterised but expensive. The intrascleral aqueous outflow tract can be visualised by OCT, however to reliably identify those vessels draining aqueous the application of a contrast agent is desireable. We tested 12% fat milk as a potential agent for this application.

Methods: OCT images were obtained with a spectral domain device for clinical use (Spectralis OCT, Heidelberg Engineering, Germany). To determine the reflectivity of candidate contrast agents, transparent plastic tubes of 5 mm diameter were filled with either balanced salt solution, black ink or high fat (12%) milk and scanned with the OCT device. Normalised 8-bit grey scale pixel values from inside the test tubes were compared between the liquids (n=8, ANOVA with Tukey post hoc testing). For an ex vivo eye imaging application the anterior chamber of bovine eyes was cannulated to perfuse the aqueous outflow tract with either BSS or milk. OCT volume scans were obtained from the intrascleral aqueous veins, using 30 frames averaging per B-scan. The same region was scanned before and after perfusion with milk. Normalised 8-bit grey value pixel intensity in aqueous veins was measured at different locations and the intensity

shift after perfusion with milk was quantified (n=8, Wilcoxon matched pairs signed rank test).
Results: In the test tubes 12% fat milk shows a significant increase in OCT reflectivity compared to BSS and ink (185±34, 0.8±1.5 and 0.9±1.0, respectively, $p<0.0001$). When applied to ex vivo imaging of aqueous veins in bovine eyes, the perfusion with milk led to a significant shift in the intraluminal reflectivity (normalised pixel intensity BSS: 4.6±3.2, milk: 138±27; $p=0.0078$) and, thus, allowed to distinguished between aqueous veins and blood vessels without connection to the anterior chamber. Despite the relatively high reflectivity of milk, no shadow was cast from the milk perfused vessels, leaving the images free of the vertical stripy shadows which are seen in blood perfused vessels.
Conclusions: For ex vivo applications 12% fat milk proofed a low-cost and effective contrast agent for OCT imaging. Although not directly transferrable to in vivo application the principle of using fatty emulsions as possible contrast agents might be worth further investigation.
Commercial Relationships: Christian van Oterendorp, None; **Viktoria Mans**, None; **Charlotte Fischer**, None; **Mohammed Khattab**, None; **Thomas Wecker**, None